AGU PUBLICATIONS

JGR

Journal of Geophysical Research: Atmospheres

RESEARCH ARTICLE
10.1002/2015JD023358

Key Points:
- A regional anthropogenic black carbon emission inventory is developed for Russia
- Simulation of Arctic and Russian black carbon has been significantly improved
- The role of Russian emissions on Arctic BC is underestimated in previous studies

Supporting Information:
- Tables S1–S13, Figures S1–S9, and Text S1

Correspondence to:
J. S. Fu,
jsfu@utk.edu

Citation:
Huang, K., J. S. Fu, V. Y. Prikhodko, J. M. Storey, A. Romanov, E. L. Hodson, J. Cresko, I. Morozova, Y. Ignatieva, and J. Cabaniss (2015), Russian anthropogenic black carbon: Emission reconstruction and Arctic black carbon simulation, *J. Geophys. Res. Atmos.*, *120*, doi:10.1002/2015JD023358.

Received 9 MAR 2015
Accepted 30 SEP 2015
Accepted article online 2 OCT 2015

Russian anthropogenic black carbon: Emission reconstruction and Arctic black carbon simulation

Kan Huang[1], Joshua S. Fu[1], Vitaly Y. Prikhodko[2], John M. Storey[2], Alexander Romanov[3], Elke L. Hodson[4], Joe Cresko[4], Irina Morozova[3], Yulia Ignatieva[3], and John Cabaniss[4]

[1]Department of Civil and Environmental Engineering, University of Tennessee, Knoxville, Knoxville, Tennessee, USA, [2]Energy and Environmental Sciences Directorate, Oak Ridge National Laboratory, Oak Ridge, Tennessee, USA, [3]Scientific Research Institute for Atmospheric Air Protection, JSC, Saint-Petersburg, Russia, [4]U.S. Department of Energy, Washington, District of Columbia, USA

Abstract Development of reliable source emission inventories is particularly needed to advance the understanding of the origin of Arctic haze using chemical transport modeling. This study develops a regional anthropogenic black carbon (BC) emission inventory for the Russian Federation, the largest country by land area in the Arctic Council. Activity data from combination of local Russia information and international resources, emission factors based on either Russian documents or adjusted values for local conditions, and other emission source data are used to approximate the BC emissions. Emissions are gridded at a resolution of 0.1° × 0.1° and developed into a monthly temporal profile. Total anthropogenic BC emission of Russia in 2010 is estimated to be around 224 Gg. Gas flaring, a commonly ignored black carbon source, contributes a significant fraction of 36.2% to Russia's total anthropogenic BC emissions. Other sectors, i.e., residential, transportation, industry, and power plants, contribute 25.0%, 20.3%, 13.1%, and 5.4%, respectively. Three major BC hot spot regions are identified: the European part of Russia, the southern central part of Russia where human population densities are relatively high, and the Urals Federal District where Russia's major oil and gas fields are located but with sparse human population. BC simulations are conducted using the hemispheric version of Community Multi-scale Air Quality Model with emission inputs from a global emission database EDGAR (Emissions Database for Global Atmospheric Research)-HTAPv2 (Hemispheric Transport of Air Pollution) and EDGAR-HTAPv2 with its Russian part replaced by the newly developed Russian BC emissions, respectively. The simulation using the new Russian BC emission inventory could improve 30–65% of absorption aerosol optical depth measured at the AERONET sites in Russia throughout the whole year as compared to that using the default HTAPv2 emissions. At the four ground monitoring sites (Zeppelin, Barrow, Alert, and Tiksi) in the Arctic Circle, surface BC simulations are improved the most during the Arctic haze periods (October–March). The poor performance of Arctic BC simulations in previous studies may be partly ascribed to the Russian BC emissions built on out-of-date and/or missing information, which could result in biases to both emission rates and the spatial distribution of emissions. This study highlights that the impact of Russian emissions on the Arctic haze has likely been underestimated, and its role in the Arctic climate system needs to be reassessed. The Russian black carbon emission source data generated in this study can be obtained via http://abci.ornl.gov/download.shtml or http://acs.engr.utk.edu/Data.php.

1. Introduction

Black carbon (BC) is estimated to be the second largest contributor to global warming, about two thirds of that from carbon dioxide [*Bond et al.*, 2013]. BC depositions on the areas covered by snow and ice such as the Arctic also exert a climate warming effect by decreasing the surface albedo and promoting snowmelt [*Quinn et al.*, 2007]. The temperature response to the BC emission in the Arctic was simulated to be 0.24 K Tg^{-1} BC yr^{-1}, almost five times as large as that of 0.05 K Tg^{-1} BC yr^{-1} in the midlatitudes [*Sand et al.*, 2013]. In addition, the well-known "Arctic haze" phenomenon usually occurs from late winter to early spring accompanied by observations of enhanced aerosol concentrations and aerosol chemical species such as sulfate and BC [*Law and Stohl*, 2007; *Rahn*, 1981; *Shaw*, 1995]. Three major pathways of air pollution transport into the Arctic were identified: low-level transport followed by ascent in the Arctic, low-level transport alone, and uplift outside the Arctic, followed by descent in the Arctic [*Stohl*, 2006]. In winter, the Arctic front (polar dome) can

extend to sufficiently cold regions as low as 40°N, thus enabling the air pollutants of northern Eurasia to penetrate into the Arctic over a shorter time scale [*Arctic Monitoring and Assessment Programme (AMAP)*, 2011; *Law and Stohl*, 2007].

In regards to the important role of the Arctic in the global climate system, considerable modeling efforts have occurred during the past decade. However, the chemical transport modeling community has, for a long time, struggled to reproduce the pollutant concentrations in the Arctic, especially for particulate BC. In one modeling effort, the Danish Eulerian Hemispheric Model [*Christensen*, 1997] simulated BC concentrations at five Arctic stations (Station Nord, Alert, Zeppelin, Barrow, and Summit). The discrepancies between the measurements and the model reached up to a factor of 6 at Barrow as well as underestimations to different extents at the other sites. At Summit, the seasonal variation failed to be captured [*AMAP*, 2011]. Simulations conducted with two other global models (National Center for Atmospheric Research Community Climate System Model and Olso CTM2) performed even worse at the same five Arctic stations above given that meteorology was in the forecast mode and the inconsistency between emission inventories (year 2000) and measurements (year 2008–2009) [*AMAP*, 2011]. The AeroCom model intercomparison project found the largest divergence in northern Eurasia and the remote Arctic compared to various experimental observations [*Koch et al.*, 2009]. Simulated BC concentrations from multiple models were compared with the flight observations made during the International Polar Year. In addition to the significant discrepancy among various models, almost all the models largely biased the measured BC values. Specifically, models tended to underestimate the BC concentrations in the lower troposphere while overestimated in the upper troposphere and lower stratosphere. *Shindell et al.* [2008] also conducted an ensemble model simulation analysis compared to BC measurements at Barrow and Alert. All the models strongly underestimated BC concentrations at the two sites and failed to capture the high values during the Arctic haze periods while overestimating BC concentrations in summer. In contrast, *Sharma et al.* [2013] overestimated the BC concentrations at three Arctic sites, especially at Ny-Ålesund by using the National Institute for Environmental Studies global atmospheric transport model. Possible causes are attributed to the adoption of a higher BC fossil fuel emission factor, which was a factor of 2 higher than a previous study [*Bond et al.*, 2007], and also a longer lifetime (an average of 10.5 days) of the BC particles in the model.

To improve the model performance of black carbon over the Arctic region, most previous studies endeavor to modify the dry and wet deposition schemes, which are testified to be important parameters influencing the surface concentration, deposition, and burden of black carbon. *Liu et al.* [2011] found that by applying the surface-dependent dry deposition velocities and by reducing the wet removal efficiency of BC in ice clouds, the simulated magnitude, seasonal cycle, and vertical profile of BC over the Arctic could be significantly improved and the wintertime concentrations of BC in the Arctic were increased by a factor of 100 throughout the tropospheric column. By modifying the dry deposition, in-cloud scavenging, and below-cloud scavenging schemes in the Canadian global air quality model (Global Environmental Multiscale model with Air Quality processes), it is found that the modifications in the wet scavenging schemes of Canadian Aerosol Module (CAM) could significantly improve the seasonality of BC in the Arctic, but at the same time, overestimations were indicated at all three sites (Alert, Barrow, and Zeppelin) during different periods [*Huang et al.*, 2010]. A set of modifications was made to the wet removal scheme in the Community Atmosphere Model version 5 (CAM5), by which the Arctic BC burden could be elevated about tenfold (fivefold) in DJF (December–February) and JJA (June–August). Also, by slowing the BC aging in the seven-mode aerosol module, the Arctic DJF (JJA) BC burden showed an additional 30-fold (fivefold) increase compared to the standard CAM5. However, this slow-aging assumption overpredicted the upper tropospheric BC because wet removal was too slow and there was too much vertical transport [*Wang et al.*, 2013]. Several scenarios for modifying the wet scavenging coefficients were designed and showed big differences for the partitioning of the dry and wet deposition in the total BC deposition [*Sharma et al.*, 2013]. By changing the dry deposition velocity, the model performance could indeed be improved at some sites but could also be worsened at other sites where the BC concentrations were simulated well using the default model configuration.

Across-the-board adjustments of the model schemes may reduce biases in certain regions but could also make the model performance worse in some other regions [*Bond et al.*, 2013]. Recently, based on the country-wide emission statistics from Russian Federation [*Huang et al.*, 2014], a pilot investigation found that several Russian emission sectors, including power, gas flaring, and mining, have been significantly underestimated or even missing in the community global emission database Emissions Database for Global Atmospheric Research (EDGAR). In addition, *Stohl et al.* [2013] first introduced the residential

combustion emissions with improved temporal resolution and added gas flaring emissions. These additions improved the simulation of BC in the Arctic although discrepancies between their model and observations still existed. In that study, comments were made that previous studies incorporating modifications of certain schemes in the model were not appropriate. In addition to the model biases caused by factors such as emissions, removal rates, and vertical transport summarized by *Bond et al.* [2013], the model grid resolution could be another cause of the model bias relative to measurements. Currently, most global models are limited by relatively coarse spatial resolution, usually at the resolution of 2–3° or greater. Coarse grid simulation usually dilutes the concentrations of pollutants when compared to the site measurement, especially for remote regions like the Arctic where concentrations of BC are in the magnitude of ng/m^3. As such, regional modeling efforts with finer spatial resolution are needed for the Arctic region in future work.

Most observational studies have reached consensus on the sources of BC in the Arctic. In an early study, the source region of the Arctic haze was attributed largely to Eurasia based on the high SO_4^{2-}/V ratio of the Arctic during winter [*Rahn*, 1981]. *Hirdman et al.* [2010] conducted source identification of typical Arctic haze components using a Lagrangian particle dispersion model and measurement data at various Arctic sites during 2000–2007. In winter, equivalent BC and sulfate measured at the low-altitude stations (Zeppelin, Alert, and Barrow) are found to be highly sensitive to the emissions in high-latitude Eurasia. Particularly, sulfate has important source originating from Eastern Europe and the metal smelting industry in Norilsk, Russia. In a recent study, *Nguyen et al.* [2013] applied two source apportionment techniques based on aerosol chemical data measured at Station Nord, Greenland, during 2008–2010. It was found that high concentrations of Pb and As related to the combustion source were impacted by the large-scale industries in Siberia. BC was attributed to the Siberian origin with a very high probability of 80–98%. Another 47 year study (1964–2010) of aerosol measurements in Finland found a consistency between the trends of As, Pb, and Cd concentrations and the reported trends of European emission inventories. By using V, Mn, Mo, Sb, Se, and Tl as markers of stationary fuel combustion, the Pechora Basin and Ural industrial areas in Russia and the gas and oil fields in western Kazakhstan were diagnosed as the source regions [*Laing et al.*, 2014]. In another recent study, combining a multiyear measurement of BC concentrations at two Arctic sites (Alert Nunavut in Canada and Tiksi Bay in Russia) with the Potential Source Contribution Function method, a region south of Moscow and another region north of the Ural Mountains were found as major source regions for Arctic BC [*Cheng*, 2014].

As the country that occupies the largest area in the Arctic Circle, Russia's BC emissions are supposed to be more uncertain compared to the other Arctic Council members (i.e., Nordic countries, Canada, and United States) and Western Europe. This is mainly attributed to the lack of local BC emission factors and detailed facility-level activity data for a wide range of sources (more details are presented in section 2.1). The goal of this study is to better understand the BC emission sources in Russia and to reevaluate their impacts on the Arctic. Here we reconstruct BC emissions from five major sectors of Russia in 2010 based on available Russian local activity data, emission factors, and other information. The hemispheric version of Community Multi-scale Air Quality Model (H-CMAQ) with polar projection is performed to simulate the Arctic BC for the first time. Emission inputs from both the standard EDGAR-Hemispheric Transport of Air Pollution version 2 (HTAPv2) and the EDGAR-HTAPv2 augmented with the new Russian BC emissions are fed into the model. Our results show that the improved Russian BC emissions can enhance the capabilities of model to reproduce the BC levels in Russia as well as in the Arctic.

2. Methodology

2.1. Emission Estimates and Spatial Allocation

The principal approach to the estimation of BC emissions is based on activity data, emission factors, and the application of control technologies. The emission for a specific sector is estimated as follows [*Klimont et al.*, 2002; *Bond et al.*, 2004]:

$$\mathrm{Emi} = \sum\nolimits_{i,j} \left\{ A_{i,j} \times \mathrm{EF}_{i,j} \times \left(1 - \eta_{i,j}\right) \right\}, \tag{1}$$

where i and j represent the subcategory of a specific emission sector, and fuel or product type; A, EF, and η represents activity data (e.g., fuel consumption and vehicle fleet), the unabated emission factor, and removal efficiency (the reduction percentage of raw emissions from control technology), respectively. For sectors with available local or estimated BC emission factors for Russia, $\mathrm{EF}_{i,j}$ represents the BC emission

factor, for sectors with no appropriate local BC emission factors, $EF_{i,s}$ represents the local particulate matter (PM) emission factor. Then the PM emission is further scaled using the emission source profiles of BC/PM ratios to derive the BC emission. The methodology for each target emission sector will be explicitly described in the following sections.

The national sectoral BC emissions are allocated to grids by using GIS (geographic information system) technology. They are first allocated at the Russian federal district or provincial level, based on different types of provincial activity data or socio-economic indicators. Then the district or provincial emissions are further allocated to grid cells using appropriate proxies:

$$\mathrm{Emi}_{[i,j]} = \mathrm{Emi} \times \left(\mathrm{P1}_n / \sum \mathrm{P1}_n\right) \times \left(\mathrm{P2}_{n\ [i,j]} / \sum \mathrm{P2}_{n\ [i,j]}\right), \tag{2}$$

where $P1_n$ represents the activity data or social economic indicators of a specific emission sector in district or province n, $P2_{n\ [i,j]}$ represents a specific proxy for emission allocation at grid cell $[i,j]$ within district or province n, and $\mathrm{Emi}_{\ [i,j]}$ represents the BC emission at grid cell $[i,j]$. All sectoral emissions are finally gridded to a spatial resolution of $0.1° \times 0.1°$.

2.1.1. Gas Flaring BC Emissions

Emissions from gas flaring have rarely been considered in global/regional emission inventories [*Amann et al.*, 2013]. Flaring is a widely used approach of discharging and disposing of gaseous and liquid hydrocarbons through combustion at oil and gas production sites including oil wells, gas wells, offshore oil and gas rigs, and landfills. Significant amounts of associated petroleum gas (APG) are flared as waste for the reason of protection against the dangers of overpressurizing industrial plant equipment in those areas lacking the pipelines and other gas transportation infrastructure. Since the associated gas is being flared primarily as a safety issue, there is often little attention paid to whether the combustion is complete or incomplete. Incomplete combustion could result in emissions of products such as black carbon [*Banks*, 2012].

According to studies from *Evans and Roshchanka* [2014] and *Huang et al.* [2014], the combustion efficiencies of the associated gases in Russia's oil and gas fields are very low to moderate. As of the end of 2010, Russia was the leading country contributing to the world's gas flaring with a dominant percentage of 25.8% from NOAA's satellite data [*World Bank*, 2012]. Based on a preliminary estimate of the BC emission from flaring, its magnitude could contribute up to 12% of the total BC emissions from the Arctic Council nations in 2000, primarily originating from Russia [*AMAP*, 2011]. Among the various cryosphere regions around the globe, climate benefits (in terms of the decrease in radiative forcing) from gas flaring BC emission reduction in the Arctic showed the second largest among Himalayas, East Africa, Andes, and Antarctica [*Pearson et al.*, 2013]. However, as summarized by *McEwen and Johnson* [2012], none of the gas flaring BC emission factors documented in the available literature [e.g., *U.S. Environmental Protection Agency*, 1995; *Canadian Association and Petrolium Producers (CAPP)*, 2007] was based on measurements from actual solution gas flares and none considered the operating conditions of a flare, such as wind speed, exit velocity, detailed fuel composition, flare size, or flare tip design. Very limited field measurements of BC emission factors from gas flaring are available. By using an advanced optical technique sky Line-of-Sight Attenuation, the emission factor measured in the gas flaring field of Uzbekistan [*Johnson et al.*, 2011] and Mexico [*Johnson et al.*, 2013] was determined to be 2 ± 0.66 and 0.067 ± 0.02 g/s, respectively. The emission factors above are presented in the form of soot mass emission rate, i.e., unit in g/s. Since the gas flaring volume is usually reported in the unit of bcm (billion cubic meters), it is difficult to use the mass emission rate for the estimation of BC emission. In addition, the two studies above showed a factor of over 30 times difference for the soot mass emission rates, which was attributed to the different characteristics of flares in different regions [*Johnson et al.*, 2013]. This suggests that a representative emission factor is needed for a best estimation of the gas flaring BC emission of Russia in this study, as well as for other regions with regard to building a global gas flaring emission inventory.

McEwen and Johnson [2012] carried out the first quantitative measurements of the BC emission factors by imitating flares at the laboratory scale with consideration of different parameters, including burner diameters, exit velocities, and fuel compositions. They found that the BC emission factor had a good linear relationship with the fuel heating value and a linear regression equation is derived as follows:

$$\mathrm{EF}_{\mathrm{flare}} = 0.0578 \times \mathrm{HV}_{\mathrm{APG}} - 2.09 \ \left(\text{correlation: } R^2 = 0.85\right), \tag{3}$$

where EF_{flare} and HV_{APG} represent the gas flaring BC emission factor and the volumetric heating value. According to this equation, the heating value of APG in Russia should be determined to approximate the

Table 1. Composition of the Associated Gas in Russia During Three Separation Stages and the Heating Values of Each Component

Associated Gas Composition		Heating Value (MJ/m^3)	Volume Percentage (%)		
			Stage 1	Stage 2	Stage 3
Methane	CH_4	39.9012	61.7452	45.6094	19.4437
Ethane	C_2H_6	69.9213	7.7166	16.314	5.7315
Propane	C_3H_8	101.3231	17.5915	21.1402	4.5642
i-Butane	i-C_4H_{10}	133.1190	3.7653	5.1382	4.3904
n-Butane	n-C_4H_{10}	134.0610	4.8729	7.0745	9.6642
i-Pentanes	i-C_5H_{12}	148.4913	0.9822	1.4431	9.9321
n-Pentane	n-C_5H_{12}	141.1918	0.9173	1.3521	12.3281
i-Hexane	i-C_6H_{14}	176.8591	0.5266	0.7539	13.8146
n-Hexane	n-C_6H_{14}	177.1907	0.2403	0.2825	3.7314
i-Heptane	i-C_7H_{16}	205.0068	0.0274	0.1321	6.726
Benzene	C_6H_6	147.3980	0.0017	0.0061	0.0414
n-Heptane	n-C_7H_{16}	205.0068	0.1014	0.0753	1.5978
i-Octane	i-C_8H_{18}	232.8155	0.0256	0.0193	4.3698
Toluene	C_7H_8	373.0365	0.0688	0.0679	0.0901
n-Octane	n-C_8H_{18}	232.8155	0.0017	0.0026	0.4826
i-Nonane	i-C_9H_{20}	260.6688	0.0006	0.0003	0.8705
n-Nonane	n-C_9H_{20}	260.6688	0.0015	0.0012	0.8714
i-Decane	i-$C_{10}H_{22}$	288.4775	0.0131	0.01	0.1852
n-Decane	n-$C_{10}H_{22}$	288.4775	0.0191	0.016	0.1912
Carbon dioxide	CO_2	-	0.0382	0.1084	0.7743
Nitrogen	N_2	-	1.343	0.453	0.1995
Hydrogen sulfide	H_2S	-	0	0	0

BC emission factor. Table 1 shows the composition of APG in Russia during three stages of operation [*Filippov*, 2012], along with the heating value of each species. As shown in the table, the composition of associated gas in Russia is far from pure natural gas (i.e., methane) but is typically mixed with other hydrocarbons such as ethane, propane, butane, and pentane. According to *PFC Energy* [2007], around 75% of the Russian fields produce associated gases with methane composition less than 50%. It may be argued that this composition is representative of all the oil and gas production areas in Russia. As shown in Figure S2 in the supporting information that will be discussed later, the major oil and gas fields in Russia are limited to certain regions, e.g., the Khanty-Mansiysk Autonomous Okrug and Yamalo-Nenets Autonomous Okrug. The geological properties of those fields are similar, hence probably resulting in the production of oil and gas with similar chemical composition. This is corroborated by the field data (LUKOIL 2013 Fact Book, 2014, http://www.lukoil.com/materials/images/Reserves/2014/Perspect_FB_eng_25-29.pdf). Petroleum densities (expressed in the American Petroleum Institute gravity) at 14 fields exhibit close values as shown in Figure S1, in turn, suggesting no distinct differences of the associated gas composition among different production fields. According to the expert estimate, the fraction of APG released during Stage 3 is the lowest in the range of 10–15% due to the low-pressure separation process. As for Stages 1 and 2, the fraction is usually in the range of 50–70% and 15%–40%, respectively. The weighted volume fraction of a specific hydrocarbon compound during the whole processing (from Stage 1 to Stage 3) is calculated as below:

$$F_{HC} = \alpha_{HC,\,S1} * \beta_{S1} + \alpha_{HC,\,S2} * \beta_{S2} + \alpha_{HC,\,S3} * \beta_{S3}, \tag{4}$$

α represents the volume fraction of the APG components (*HC*) during each separation stage (*S*) as shown in Table 1; β represents volume contributions during the three separation stages. Then, the weighted APG heating value is calculated as follows:

$$\mathrm{HV_{APG}} = \sum \mathrm{HV}_{HC} * F_{HC}, \tag{5}$$

Since β_{S1}, β_{S2}, and β_{S3} are all within some certain ranges, there are multiple combinations of these three parameters. We assume different values for β_{S1}, β_{S2}, and β_{S3} with 1% interval; i.e., β_{S3} is in [10%, 11%, …. 15%], β_{S1} is in [50%, 51%, …. 70%], and $\beta_{S2} = 1 - \beta_{S1} - \beta_{S3}$. Then a range of $\mathrm{HV_{APG}}$ values could be obtained as shown in Figure S3. The calculated $\mathrm{HV_{APG}}$ values span from around 73–78 MJ/m^3, much higher than that of the pure natural gas (i.e., methane of 39.9 MJ/m^3). The median value of those $\mathrm{HV_{APG}}$ values is calculated

to be 75.5 MJ/m^3 and is used as input to derive the BC emission factor from gas flaring. By using equation (3), the BC emission factor from gas flaring in Russia is estimated to be 2.27 g/m^3. This value is slightly lower than that of 2.56 g/m^3 from *CAPP* [2007], but higher than that of 1.6 g/m^3 from *Stohl et al.* [2013] and 0.51 g/m^3 from *McEwen and Johnson* [2012]. Although the experimental data used to develop the linear relationship in equation (3) only range as high as 47 MJ/m^3, for this study, the linear function was extrapolated to a HV of 75.5 MJ/m^3, thus exceeding the experimental range. Hence, the gas flaring emission factor estimated in this study is regarded as highly uncertain unless field measurements or laboratory experiments with gas flares burning heavier fuel compositions become available in the future. The sooting tendencies of heavier fuel flames are particularly sensitive to air-fuel ratio, so this study identifies an important future need to specifically understand Russian gas flaring BC emissions, due to the heavier gas composition.

The annual volumes of national gas flaring are estimated using low light imaging data from the U.S. Air Force Defense Meteorological Satellite Program (DMSP) [*Elvidge et al.*, 2009]. A linear regression model is fitted between the reported volume of flared gas available from various countries and "sum of lights index," i.e., bcm = 0.0000266 × sum of lights index, $R^2 = 0.976$. Sum of lights index refers to the nighttime lights product, which is calculated from the average visible band digital number of cloud-free light detections multiplied by the percent frequency of light detection. By using this equation, volumes of flared gas for individual countries are predicted. As for Russia, it is hard to verify the volume of flared gas which is retrieved from satellite. According to *PFC Energy* [2007], in Russia, there is little incentive for accurate metering of associated gas utilization and flaring due to the lack of gas utilization requirements under many licenses. The accuracy of reported flaring figures is not regularly monitored by government agencies. Hence, it is impossible to estimate how much gas is vented and flared under the current technical standards implemented in Russia. In this regard, satellite retrieval is the only available source of flared gas volume in Russia at the time of this study. In 2010, based on the sum of light index, the total volume of gas flaring in Russia was estimated to reach 35.6 bcm. By multiplying the gas flaring volume and the calculated BC emission factor above, the BC emissions from gas flaring in Russia can be estimated.

To distribute the total gas flaring BC emission into grid cells, the nighttime lights product referred above is used as the proxy. The values of lights index at the 1 km^2 grid cells range from 0 to ~60, and its spatial distribution is shown in Figure S2. Gas flares are identified as the sum of lights index values of 8.0 or greater for all the 1 km^2 grid cells [*Elvidge et al.*, 2009]. Hence, the locations of gas flaring areas in Russia can be identified and marked by the red polygons shown in Figure S2. Khanty-Mansiysk Autonomous Okrug, Yamalo-Nenets Autonomous Okrug, Komi Republic, Nenets Autonomous Okrug, and Tomsk Oblast are the major flaring regions of Russia (see names in Figure S2). It should be noted that the gas flares mainly occurred in the remote areas of Russia with very sparse human population density (Figure S4). Thus, the interference from the residential lights will be minimized. The national gas flaring BC emission can be allocated as below:

$$BC_{i,j} = BC_{flaring} \times L_{i,j} / \sum \left(L_{i,j}\right), \tag{6}$$

where $BC_{flaring}$ is the Russian national gas flaring BC emission, $L_{i,j}$ is the nighttime light intensity product (avg_lights_x_pct) at grid cell [*i,j*], and $BC_{i,j}$ is the BC emission at grid cell [*i,j*].

2.1.2. Transportation BC Emissions

BC emissions from the transportation sector considered in this study include the hot emissions during normal driving operation and also the emissions from cold starts. It should be noted that the transportation sector does not include the nonroad transportation, e.g., haul trucks and mining equipments applied in the mining industries, locomotives, construction vehicles, agricultural machinery, etc. *Evans et al.* [2015] conducted a bottom-up diesel BC emission study for the Murmansk Oblast and Murmansk City, the largest city above the Arctic Circle. However, emission factors for the nonroad sector in their study are based on the European Monitoring and Evaluation Programme/European Environment Agency (EMEP/EEA) emission guidebook but not local values. Input data for various sectors of the nonroad transportation are often difficult to obtain for the whole Russian Federation. In addition, we lack suitable proxies to spatially allocate these nonroad emissions. In this regard, BC emissions from the nonroad transportation are not considered in the current study.

2.1.2.1. Road Transportation BC Emissions

In regard of the road transportation, vehicles are classified into public transportation and nonpublic transportation according to Russia's transportation methodological guidelines (http://www.gks.ru/bgd/regl/b14_12/IssWWW.

exe/stg/d02/18-00.htm). BC emission from transportation is estimated based on the vehicle annual mileages traveled and BC emission factors (unit: g/km) depending on different vehicle types, road conditions, and emission standards. Since the vehicle mileage is not directly reported from any literature, reports, or the Russian government statistics, it is estimated using the following equation:

$$\mathrm{VMT}_v = (\mathrm{TO}_v/N_v) \times J_v/S_v, \tag{7}$$

where VMT_v is the annual mileage traveled for the vehicle type v; TO_v is the annual passenger or cargo turnover (unit: passenger-kilometers or tons-kilometers) of the vehicle type v; N_v is the annual number of passengers or weight of cargo of the vehicle type v; thus, TO_v/N_v represents the average distance of transporting passenger or cargo during one journey; J_v is the annual number of journeys of the vehicle type v; and S_v is the vehicle stock of the vehicle type v.

Table S1 in the supporting information lists the transportation statistics of Russia in 2010. The passenger turnover, total passengers carried, and the number of journey are reported from Russia's Federal State Statistics Service (FSSS) only for the public transportation. Thus, the annual mileages of public buses (categorized into three groups of intercity, suburban, and urban) and taxi are calculated according to equation (7) and the values are shown in the last column of Table S1. For cars (including company-owned and private) and private buses, there is not enough information available for estimating their mileages. Thus, empirical mileage data for cars and private buses are used in this study according to the Ministry of Transport of the Russian Federation Research Institute [*Ministry of Transport of the Russian Federation Research Institute (MTRFRI)*, 2008]. As for the freight vehicles, although the data of cargo turnover and weight are available, the lacking of journey number makes the estimation of mileage difficult. Hence, the empirical mileage data for the freight vehicle from *MTRFRI* [2008] are also applied. It should be noted that the mileage provided by *MTRFRI* [2008] has certain ranges. In the emission estimations below, the median values will be used.

The black carbon emission during the hot operation stage (i.e., driving mode) is calculated as follows:

$$\mathrm{Emi}_{\mathrm{hot}} = \sum \mathrm{EF}_{\mathrm{PM},ijk} \times \left(S_{ij} \times \mathrm{Eu}_{ijk} \times R_{ij} \times \mathrm{VMT}_{ijk}\right) \times (\mathrm{BC}/\mathrm{PM}_{2.5})_{ijk}, \tag{8}$$

where i, j, and k represent the vehicle type, driving condition, and Euro standard, respectively. $\mathrm{EF}_{\mathrm{PM},\,ijk}$ is the PM emission factor depending on different vehicle types, driving conditions, and Euro standards; S_{ij} is the total vehicle stock number of vehicle type i and driving condition j; Eu_{ijk} is the percentage share of vehicles with different Euro standards k; R_{ij} is the annual usage ratio; VMT_{ijk} is the annual driving mileage per vehicle; $(\mathrm{BC}/\mathrm{PM}_{2.5})_{ijk}$ is the emission mass ratio of BC in $\mathrm{PM}_{2.5}$; and $\mathrm{Emi}_{\mathrm{hot}}$ is the annual total BC emission during the hot operation stage.

The local PM emission factors (EF_{ijk}, in units of g/km) for Russia are listed in Table S2 from the Ministry of Transport of the Russian Federation Research Institute [*MTRFRI*, 2008]. As shown in the table, the PM emission factors are categorized into four vehicle groups (cars, light-duty trucks and buses, buses, and heavy-duty trucks) with subcategories of four Euro standards (Euro 0–Euro 3) under five driving conditions, respectively. To be consistent with the driving modes shown in Table S1, the original PM emission factors in the five categories of driving conditions are further narrowed down to three categories—urban, suburban, and intercity—based on the similarity of some categories (see footnotes in Table 2). The percentage distributions of different Euro standards within each vehicle category are formatted as shown in Table S3 based on various sources, e.g., Russia's FSSS, the Russian Automotive Market Research, and other statistics.

The input parameters for estimating the black carbon emission from on-road hot operation transportation are then compiled in Table 2 based on Tables S1–S3. The last column of Table 2 represents the emission mass ratios of $\mathrm{BC}/\mathrm{PM}_{2.5}$ from the EMEP/EEA air pollutant emission inventory guidebook [*European Environment Agency* (*EEA)*, 2013b], which is used for scaling the PM emission to BC emission.

2.1.2.2. Warm-up BC Emission From Cold Start

The pollutant emission from cold start is caused by warming the engine in all climate conditions. Cold starts release more emissions in colder weather, especially for countries such as Russia. As opposed to the road transportation emission, which is estimated by using the driving mileage in section 2.1.2.1, the emissions from cold start depend on the duration of the warm-up process. The estimation of warm-up emission is shown below as similar as a city-scale study in Russia [*Evans et al.*, 2015]:

$$\mathrm{Emi}_{\mathrm{cold}} = \mathrm{EF}_{\mathrm{PM},ikl} \times (S_i \times \mathrm{Eu}_i \times R_i \times T_l) \times (\mathrm{BC}/\mathrm{PM}_{2.5})_{ik}, \tag{9}$$

Table 2. Input Parameters for Estimating the BC Emission From Road Transport, Including Readjusted PM Emission Factors, Percentage Distribution of Vehicles With Different Euro Standards, and the $BC/PM_{2.5}$ Ratios Under Three Main Driving Modes (Urban, Suburban, and Intercity)

Vehicle Type		Driving Modes	Fuel Class	[a]PM EF (g/km)	Euro Share (%)	Vehicle Stock (10^3)	Stock Use Ratio (%)	Mileage (km)	[b]$BC/PM_{2.5}$ (%)
Public buses		Urban	Euro 0	1.57	27.7	39.7	74.5	18544	50
			Euro 1	0.965	41.7				65
			Euro 2	0.755	18.7				65
			Euro 3	0.26	12.0				70
		Suburban	Euro 0	1.43	27.7	19.7	69.6	34933	50
			Euro 1	0.74	41.7				65
			Euro 2	0.53	18.7				65
			Euro 3	0.23	12.0				70
		Intercity	Euro 0	0.465	27.7	8.1	67.9	60256	50
			Euro 1	0.355	41.7				65
			Euro 2	0.29	18.7				65
			Euro 3	0.125	12.0				70
Private buses	Small	Urban	Euro 0	0.56	29.7	124.0	50.0	45000	55
			Euro 1	0.485	41.3				70
			Euro 2	0.225	16.0				80
			Euro 3	0.15	13.0				85
		Suburban	Euro 0	0.51	29.7	203.6	50.0	45000	55
			Euro 1	0.42	41.3				70
			Euro 2	0.21	16.0				80
			Euro 3	0.13	13.0				85
		Intercity	Euro 0	0.19	29.7	11.4	50.0	45000	55
			Euro 1	0.125	41.3				70
			Euro 2	0.08	16.0				80
			Euro 3	0.08	13.0				85
	Medium	Urban	Euro 0	1.255	29.7	85.2	50.0	45000	50
			Euro 1	0.875	41.3				65
			Euro 2	0.6	16.0				65
			Euro 3	0.26	13.0				70
		Suburban	Euro 0	1.14	29.7	139.9	50.0	45000	50
			Euro 1	0.76	41.3				65
			Euro 2	0.53	16.0				65
			Euro 3	0.23	13.0				70
		Intercity	Euro 0	0.375	29.7	7.9	50.0	45000	50
			Euro 1	0.32	41.3				65
			Euro 2	0.29	16.0				65
			Euro 3	0.125	13.0				70
	Large	Urban	Euro 0	1.57	29.7	32.1	60.0	45000	50
			Euro 1	0.965	41.3				65
			Euro 2	0.755	16.0				65
			Euro 3	0.26	13.0				70
		Suburban	Euro 0	1.43	29.7	52.7	60.0	45000	50
			Euro 1	0.74	41.3				65
			Euro 2	0.53	16.0				65
			Euro 3	0.23	13.0				70
		Intercity	Euro 0	0.465	29.7	3.0	60.0	45000	50
			Euro 1	0.355	41.3				65
			Euro 2	0.29	16.0				65
			Euro 3	0.125	13.0				70
Light trucks and buses (<3.5 t)		Urban	Euro 0	0.295	51.7	490.5	60.0	35000	55
			Euro 1	0.09	29.7				70
			Euro 2	0.09	10.7				80
			Euro 3	0.06	8.0				85
		Suburban	Euro 0	0.28	51.7	805.4	60.0	35000	55
			Euro 1	0.08	29.7				70
			Euro 2	0.08	10.7				80
			Euro 3	0.05	8.0				85
		Intercity	Euro 0	0.22	51.7	45.2	60.0	35000	55
			Euro 1	0.08	29.7				70
			Euro 2	0.08	10.7				80

Table 2. (continued)

Vehicle Type		Driving Modes	Fuel Class	[a]PM EF (g/km)	Euro Share (%)	Vehicle Stock (10^3)	Stock Use Ratio (%)	Mileage (km)	[b]$BC/PM_{2.5}$ (%)
			Euro 3	0.05	8.0				85
Heavy-duty trucks	<7.5 t	Urban	Euro 0	0.565	87.5	941.5	60.0	35000	50
			Euro 1	0.37	8.5				65
			Euro 2	0.225	1.6				65
			Euro 3	0.155	2.4				70
		Suburban	Euro 0	0.5	87.5	1546.1	60.0	35000	50
			Euro 1	0.34	8.5				65
			Euro 2	0.21	1.6				65
			Euro 3	0.15	2.4				70
		Intercity	Euro 0	0.18	87.5	86.8	60.0	35000	50
			Euro 1	0.14	8.5				65
			Euro 2	0.08	1.6				65
			Euro 3	0.06	2.4				70
	7.5–16 t	Urban	Euro 0	0.95	85.7	341.7	60.0	35000	50
			Euro 1	0.655	8.6				65
			Euro 2	0.24	2.3				65
			Euro 3	0.155	3.4				70
		Suburban	Euro 0	0.78	85.7	561.1	60.0	35000	50
			Euro 1	0.61	8.6				65
			Euro 2	0.21	2.3				65
			Euro 3	0.15	3.4				70
		Intercity	Euro 0	0.4	85.7	31.5	60.0	35000	50
			Euro 1	0.33	8.6				65
			Euro 2	0.1	2.3				65
			Euro 3	0.06	3.4				70
	>16 t	Urban	Euro 0	1.215	60.7	201.4	60.0	35000	50
			Euro 1	0.785	21.2				65
			Euro 2	0.3225	7.2				65
			Euro 3	0.22	10.9				70
		Suburban	Euro 0	1.11	60.7	330.7	60.0	35000	50
			Euro 1	0.715	21.2				65
			Euro 2	0.305	7.2				65
			Euro 3	0.2	10.9				70
		Intercity	Euro 0	0.64	60.7	18.6	60.0	35000	50
			Euro 1	0.48	21.2				65
			Euro 2	0.18	7.2				65
			Euro 3	0.13	10.9				70
[c]Cars		Urban	Euro 0	0.25	46.6	11932.4	50.0	15000	20
			Euro 1	0.075	24.7				25
			Euro 2	0.075	10.3				25
			Euro 3	0.055	18.4				15
		Suburban	Euro 0	0.25	46.6	19593.7	50.0	15000	20
			Euro 1	0.07	24.7				25
			Euro 2	0.07	10.3				25
			Euro 3	0.05	18.4				15
		Intercity	Euro 0	0.16	46.6	1099.6	50.0	15000	20
			Euro 1	0.045	24.7				25
			Euro 2	0.045	10.3				25
			Euro 3	0.03	18.4				15

[a]The original PM emission factors (Table S2) are further grouped in three categories. The EFs of "I.P" and "I.MP" are averaged to represent "Urban." The EFs of "III" and "IV" are averaged to represent "Intercity." "II" represents "Suburban."

[b]Values derived from the EMEP/EEA air pollutant emission inventory guidebook - 2013, Part B: sectoral guidance chapters: 1.A.3.b. i–iv Exhaust emissions from road transport, published in 29 August 2013. For cars, lower $BC/PM_{2.5}$ ratios (15%–25%) are used. For the other vehicle categories, $BC/PM_{2.5}$ ratios from diesel combustion are used.

[c]Company-owned cars are not shown in this table, but their BC emissions are accounted into the total transportation emissions.

Journal of Geophysical Research: Atmospheres

10.1002/2015JD023358

Table 3. The Warm-up PM Emission Factors, Vehicle Stock Numbers, Annual Warm-up Time, and the Ratios of BC in $PM_{2.5}$ for Each Vehicle Category and Different Emission Standards (Euro 0 and Euro 1+)

		Subcategories	[a]Warm-up PM Emission Factors (g/min)					Annual Warm-up Time (min)			
Vehicle Type	Emission Standards	Engine Volume	Warm Season	Cold Season	Transition Season	Euro Ratio (%)	Stock Number (10^3)	Warm Season	Cold Season	Transition Season	[b]$BC/PM_{2.5}$ (%)
Cars	Euro 0	<1.4	0.002	0.004	0.0036	46.6	34372	1098	9417	372	30.0
		1.4–2.0	0.003	0.006	0.0054						
		>2.0	0.005	0.01	0.009						
		Mean	0.003	0.007	0.006						
	Euro 1 +	<1.4	0.001	0.002	0.0018	53.4	34372	549	4708.5	186	21.5
		1.4–2.0	0.002	0.003	0.0027						
		>2.0	0.003	0.005	0.0045						
		Mean	0.002	0.003	0.003						
Trucks and buses (<3.5 t)	Euro 0		0.01	0.04	0.036	51.7	1341	976	9542	372	55.0
	Euro 1+		0.005	0.01	0.009	48.3	1341	976	9542	372	74.7
Trucks (>3.5 t)		Weight									
	Euro 0	<7.5 t	0.01	0.04	0.036	87.5	2575	976	9542	372	50.0
		7.5–16 t	0.02	0.08	0.072	85.7	934	976	9542	372	50.0
		16–32 t	0.03	0.12	0.108	60.7	551	976	9542	372	50.0
	Euro 1 +	<7.5 t	0.008	0.016	0.0144	12.5	2575	976	9542	372	65.9
		7.5–16 t	0.012	0.024	0.0216	14.3	934	976	9542	372	66.2
		16–32 t	0.019	0.038	0.0342	39.3	551	976	9542	372	66.4
		>32 t	0.023	0.046	0.0414						
Buses (>3.5 t)		Size									
	Euro 0	Small	0.02	0.08	0.072	29.7	339	976	9542	372	50.0
		Medium	0.03	0.12	0.108	29.7	233	976	9542	372	50.0
		Large	0.04	0.16	0.144	29.7	88	976	9542	372	50.0
	Euro 1+	Small	0.007	0.014	0.0126	70.3	339	976	9542	372	65.9
		Medium	0.016	0.032	0.0288	70.3	233	976	9542	372	65.9
		Large	0.02	0.04	0.036	70.3	88	976	9542	372	65.9
		Very large	0.02	0.04	0.036						

[a]Warm-up PM emission factors (g/min) during the warm and cold seasons are derived from the Ministry of Transport of the Russian Federation Research Institute. The PM emission factors during the transition period should be multiplied by a factor of 0.9 based on the values of the cold season.

[b]Values derived from the EMEP/EEA air pollutant emission inventory guidebook - 2013, Part B: sectoral guidance chapters: 1.A.3.b. i–iv Exhaust emissions from road transport, published in 29 August 2013. For the $BC/PM_{2.5}$ ratios of the vehicles with Euro 1 and higher standards, the weighted values are calculated based on the share of different Euro standards listed in Table S3.

Table 4. Residential Fuel Types and Consumption With Corresponding Black Carbon Emission Factors

Residential Fuel	Unit	Quantity[a]	BC EF[b]
Charcoal	Metric tons, thousand	74	0.75[d]
Coke-oven coke	Metric tons, thousand	33	0.007[e]
Gas-diesel oils	Metric tons, thousand	5702	0.09[d]
Coal	Metric tons, thousand	6082	3.05[e]
Industrial waste	Terajoules	5546	4.18E-04[f]
Kerosene	Metric tons, thousand	0	0.12[f]
Lignite brown coal	Metric tons, thousand	1636	2.28[d]
Lignite-brown coal briquettes	Metric tons, thousand	8	0.09[e]
Liquefied petroleum gas (LPG)	Metric tons, thousand	3230	0.068[f]
Natural gas (including LNG)	Terajoules	2047787	9.48E-08[f]
Peat (for fuel use)	Metric tons, thousand	19	0.67[d]
Refinery gas	Metric tons, thousand	0	0.0001[f]
Residual fuel oil	Metric tons, thousand	838	0.09[d]
Fuelwood[c]	Metric cubic meters, thousand	46823.9	1.49[g]

[a]United Nations Statistics Division (version v0.14.6 Beta).
[b]All BC emission factors are in the units of g/kg except for industrial waste and natural gas are in the units of tons/terajoules.
[c]Fuelwood consumption data are based on Russia's FSSS. For tree species typical in Russia, 1 m^3 of wood equals to 0.5 t of dry biomass [*Izrael et al.*, 1997].
[d]*Junker and Liousse* [2008].
[e]*Chen et al.* [2009].
[f]*Bond et al.* [2004].
[g]*Li et al.* [2009].

where l represents three season categories, i.e., warm, cold, and the transition season; T_l represents the total warming time during the season l; $EF_{PM,ikl}$ represents the PM emission factor depending on vehicle type i, Euro standard k, and the season l, in units of g/min; and the other parameters have been defined in section 2.1.2.1.

Table S4 shows the warm-up time depending on the different ranges of the ambient temperature per day per vehicle as well as the number of cold starts per day and the stock use ratio based on [*MTRFRI*, 2008]. Table S5 further estimates the daily total warm-up time per vehicle based on the average temperature of each month in 2010. Finally, Table 3 summarizes all the parameters used for calculating the black carbon emission from cold starts.

2.1.3. Residential BC Emissions

Black carbon emissions from residential sources are estimated from various fuel types, emission factors, and removal efficiencies. Table 4 lists the annual consumption of different types of fuels in Russia in 2010 and the corresponding BC emission factors. Both fossil fuels and biofuels are consumed in the households. The fossil fuels mainly include coal (raw coal, light brown coal, and briquettes), oil (kerosene, residual fuel oil, and liquefied petroleum gas), gases (natural gas and refinery gas), and coke-oven coke, and the biofuels include firewood, peat, and charcoal. It should be noted that no local BC or PM emission factors for the residential sector in Russia are available; thus, we adopt emission factors from adjacent countries with similar economic development from *Bond et al.* [2004], *Chen et al.* [2009], *Junker and Liousse* [2008], and *Li et al.* [2009]. It should be noted that the adoption of foreign emission factors is a temporary solution. For instance, emission factor for fuelwood BC is adopted from a Chinese study [*Li et al.*, 2009], due to some similarities of stoves used in Russia and China. Historically, people have been using masonry heating for centuries in Northeastern Europe and Asia and the Russians and Chinese have used a similar sort of stove. A Russian oven is designed by channeling the smoke and hot air produced by combustion through the masonry passages. The bricks from which the oven is constructed are warmed to retain heat for long periods of time. In China, this sort of stove has been widely used in households. Besides its use for domestic heating, in winter people may sleep on top of the oven to keep warm. This is as similar as the heated bed floor in China which is the so-called "kang." In *Li et al.* [2009], the measurements were mainly conducted in the households of northern China, which is geographically close to Russia. Hence, adoption of this emission factor should provide a reasonable estimate. However, to more reasonably estimate the residential sector in Russia, field emission measurements are needed for typical stoves used in Russia in the future studies. Information of the technology divisions in Russia is obtained from *Bond et al.* [2004].

Table 5. The 2010 Raw PM Emission From the Three Subcategories of the Power Generation and Heating Sector With Their Associated Removal Efficiencies

Power Plants Sector	[a]PM Emission (Gg)	[a]Removal Efficiency (%)
Electricity production	24292.676	96.5
Transmission and distribution of steam and hot water	1903.862	82.9
Collection, purification, and distribution of water	86.41	90.2

[a]Data source: Russia's Federal State Statistics Service (FSSS).

The total residential BC emission is allocated by using equation (2). Quantities of fuel wood consumption at the Russian federal district level are reported from Russia's FSSS. Figure S5 shows the ratio of fuel wood consumption in the whole nation for each district. We first use this ratio as a proxy to distribute the total residential BC emission to the federal district level. Afterward, we further distribute the BC emission to grid resolution based on the rural human population density within each district. Human population density data are from Oak Ridge National Laboratory's (ORNL) LandScan (http://www.ornl.gov/landscan/) community standard global population data set (2010) with a very fine resolution of approximately 1 km^2 (Figure S4).

2.1.4. Power Generation and Heating BC Emissions

According to a survey of pollutant emissions from a limited number of thermal power plants in Moscow, Russia, with capacities of less than 30 t/h of steam [*Office of Technological and Environmental Surveillance*, 2005], the raw black carbon emission factor calculated from each power plant with its main fuel of oil, lignite, and coal reached 1.1, 7.1, and 6.1 g/kg, respectively. Unexpectedly and surprisingly, BC emission factors for the Russian power plants are extremely high as compared to the values from other regions of the world [*Bond et al.*, 2004; *Junker and Liousse*, 2008; *Streets et al.*, 2001; *Kupiainen and Klimont*, 2007; *Schaap et al.*, 2004]. Thus, it is not appropriate to apply the literature values for estimating BC emission from power plants in Russia. However, it is also not recommended to use the BC emission factors referred above as the universal values because these values are derived only from several small plants. In balance, the best way to develop the BC emissions from power plants is to apply the speciation ratio on an existing PM emission inventory.

Based on the methodology "Calculation methods used in Russia to estimate PM/soot emissions from power plants and boilers" (see Text S1 in the supporting information) certified by Scientific Research Institute of Atmospheric Air Protection [*Scientific Research Institute of Atmospheric Air Protection (SRI-Atmosphere)*, 2012], the 2010 PM emissions from thermal power plants are reported from Russia's FSSS. Table 5 shows the raw PM emission from three power subcategories with their associated removal efficiencies. It should be noted that the PM emissions reported from FSSS do not differentiate size distributions and should be regarded as TSP (total suspended particles). To begin with, the PM emissions are scaled to $PM_{2.5}$ emissions by using the $PM_{2.5}$/TSP ratio of 0.286, which was calculated based on an average of multiple emission factors for $PM_{2.5}$ and TSP from coal combustion in power plants [*EEA*, 2013a]. Second, it is essential to determine the fuel types of power plants in Russia. According to *International Energy Agency (IEA)* [2012], the percentage of CO_2 emission from coal, oil, and natural gas to the total from Russia's thermal power plants was 38.3%, 4.1%, and 57.6%, respectively. Since natural gas is a clean gaseous fuel with very low BC emission factor and the contribution from oil combustion to CO_2 emission is only around 4%, BC emissions from power plants are assumed to be fully attributed to the coal-fired power plants. Third, to estimate BC emissions based on $PM_{2.5}$ emissions, the PM speciation source profiles from U.S. EPA's SPECIATE database (http://www.epa.gov/ttn/chief/software/speciate/) are applied. According to *Grammelis et al.* [2006], coal-fired power plants in Russia are mainly equipped with electrostatic precipitators (ESP), scrubbers, and combinations of those equipments. By selecting the emission measurements of coal-fired power plants equipped with ESP and scrubbers, a total of 32 profiles (3 profiles are excluded as outliers) from the SPECIATE database fit our requirements. Finally, the mean value of those selected profile is used to estimate the BC emission from the power sector, and the mean ratio of BC in $PM_{2.5}$ from coal-fired power plants is 3.57%. Hence, the total BC emission emitted into the atmosphere from power plants is calculated by using the equation as below:

$$BC_{power} = \left(\sum PM_{raw,i} \times (1 - \eta_i)\right) \times \sigma_1 \times \sigma_2, \quad (10)$$

where $PM_{raw,\ i}$ represents the particulate matter emission prior to technology controls; i and η represent different subsectors and related removal efficiency, respectively; σ_1 and σ_2 represents the emission mass

Table 6. The 2010 Raw PM Emissions From Various Subcategories of Industries With Corresponding Removal Efficiencies and Ratios of BC/PM

Industry Sector	[a]PM Emission (Gg)	[a]BC/PM (%)	[a]Removal Efficiency (%)
Manufacture of food products, including beverages and tobacco	445.68	16.3	94.1
Textile and clothing manufacture	9.81	25.5	81.7
Manufacture of leather, leather goods, and footwear	1.23	32.8	70.0
Manufacture of wood and wood products	730.90	32.2	97.7
Pulp and paper production, publishing, and printing	744.95	1.4	94.8
Manufacture of coke and refined petroleum	132.79	41.3	89.0
Chemical production	2426.41	4.6	98.7
Manufacture of rubber and plastic products	8.84	15.8	87.1
Manufacture of other nonmetallic mineral products	7878.74	1.0	98.1
Basic metals and fabricated metal products	12061.32	2.1	97.8
Manufacture of machinery	65.95	10.8	76.0
Manufacture of electrical, electronic, and optical equipment	28.50	5.8	83.4
Vehicles and equipment production	66.81	8.3	75.8
Other production	60.82	12.2	92.3

[a]Data source: Russia's Federal State Statistics Service (FSSS).

ratio of $PM_{2.5}$/TSP and BC/$PM_{2.5}$, respectively; and BC_{power} represents the total BC emission from power plants after technology controls.

It should be noted that this method is a temporary solution. Specific measurements are needed for BC emissions from larger installations, especially using heavy fuel oil or Mazut (a heavy, low-quality fuel oil manufactured in the Russian Federation). Also, size distribution measurements are needed to quantify the submicron and larger fractions of black carbon.

The spatial allocation of the total BC emissions from power plants is based on a global power plant database, called CARMA (Carbon Monitoring for Action, http://www.carma.org), which contains information about the energy capacity, intensity, carbon emission, and locations of the power plants worldwide [*Wheeler and Ummel*, 2008]. To distinguish the coal-fired power plants from power plants using other fuels such as oil and natural gas, the intensity (kilograms of CO_2 emitted per MWh) of a power plant is used. Defined by CARMA (http://carma.org/blog/glossary/abouticons/) and empirical values from *IEA* [2012], the intensity of a power plant higher than 0.9 t CO_2/MWh is probably using coal as its major fuel. By using this criterion, the percentage of CO_2 emission from the coal-fired power plants in the total thermal power plants is 39.2%, very close to that of 38.3% as reported by *IEA* [2012]. After sorting out the coal-fired power plants, the BC emission from each power plant is assumed to be proportional to its CO_2 emission, i.e.,

$$BC_j = \left(CO_{2,j} / \sum CO_{2,j}\right) \times BC_{power}, \tag{11}$$

where j represents an individual power plant and BC_j and $CO_{2,j}$ represent its annual BC_{power} emission and CO_2 emission, respectively.

2.1.5. Industrial BC Emissions

Similar to the power sector, we use the same method to estimate the BC emission from industries. The particulate matter emissions from combustion in industrial boilers are also available from Russia's FSSS. Table 6 lists the raw PM emissions from various industrial sectors in 2010 with corresponding removal efficiencies. Specifically, the raw BC/PM ratios depending on different industrial sectors are also available from Russia's FSSS as shown in Table 6. The methodology of emission estimation from industrial boilers is also documented in Calculation methods used in Russia to estimate PM/soot emissions from power plants and boilers [*SRI-Atmosphere*, 2012] (see Text S1). By applying equation (10), the total BC emissions from industries could be reasonably estimated as all the input parameters are based on local information.

The national total BC emission from industries is first distributed into 83 subjects of the Russian Federation, including 46 Oblasts, 21 Republics, 9 Krais, 4 Autonomous Okrugs, 2 Federal cities, and 1 Autonomous Oblast. The annual revenue from industrial production at each federal subject is used as the proxy [*FSSS*, 2011]. It is assumed that the industrial BC emissions of each subject is proportional to its annual revenue. Figure S6 shows the percentage of industrial revenues for each Russian federal subject. Since the information

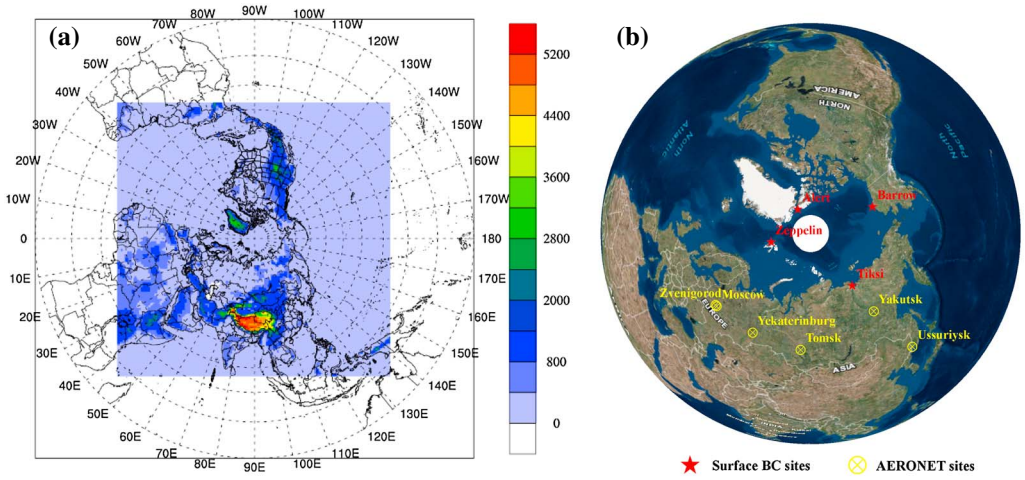

Figure 1. (a) The H-CMAQ modeling domain as indicated by the contour of the terrain height (m). (b) Four surface BC measurement sites (Barrow, Alert, Zeppelin, and Tiksi) in the Arctic Circle and six AERONET sites (Moscow, Zvenigorod, Yekaterinburg, Tomsk, Yakutsk, and Ussuriysk) in Russia.

of precise location of each industry in Russia is not available, it is further assumed that industries are located close to the areas with denser human population as workers tend to live nearby their workplaces. Thus, in this study the industrial emissions are treated as diffuse emission similar to that of residential emissions. The BC emissions within each federal subject are spatially allocated using ORNL's LandScan population density within the same federal subject.

2.2. Model Evaluation for Black Carbon Emission Inventory

The Community Multi-scale Air Quality Model (CMAQ) [*Byun and Schere*, 2006] is used to assess the new Russian black carbon emission inventory developed in this study. With focusing on the high latitudinal regions including the Arctic, the hemispheric version of CMAQ (H-CMAQ) is applied encompassing the northern hemisphere with a Polar Stereographic projection [*Mathur et al.*, 2012]. The spatial horizontal resolution is set as 108 km × 108 km with 180 × 180 grid cells, and the domain coverage is shown in Figure 1a. Compared to most of the global models which use the latitude/longitude projection, the polar projection applied in this study ensures that the North Pole region is least distorted. The vertical layers extend from the surface to 50 mb with 44 layers. CMAQv5.0.1 is configured with CB05 chemical mechanism and AER06 aerosol module. CMAQ is driven by the Weather Research and Forecasting (WRF) meteorology model version 3.5.1 with the same projection. As inputs for the WRF Preprocessing System, the National Centers for Environmental Prediction Final Analyses data set (ds083.2) are used with a resolution of 1.0° × 1.0° for every 6 h. A Meteorology/Chemistry Interface Processor 4.1 is used to link the WRF outputs to CMAQ.

The global anthropogenic emission inventory used as input for the model is the 2010 EDGAR (Emission Database for Atmospheric Research)-HTAPv2 (Hemispheric Transport of Air Pollution) data set (http://edgar.jrc.ec.europa.eu/htap_v2/index.php?SECURE=123). This is a monthly emission database with a resolution of 0.1° × 0.1°. It consists of aircraft, ship, energy, industry, transportation, residential, and agriculture sectors. Emission species include CO, SO_2, NO_x, NMVOC, NH_3, PM_{10}, $PM_{2.5}$, BC, and OC. In addition to the simulation using EDGAR-HTAPv2, we also replace the Russian part of EDGAR-HTAPv2 with the newly developed Russian BC emission in this study for simulation. Biomass burning emissions are from the Global Fire Emissions Database (GFEDv4s, http://www.globalfiredata.org/index.html). It is an updated version of *van der Werf et al.* [2010] with a spatial resolution of 0.25° × 0.25°. Conversions from biomass burning carbon emissions to various species are based on emission factors from *Andreae and Merlet* [2001].

The meteorological fields (wind speed, temperature, and humidity) simulated by WRF are evaluated against the NOAA National Climate Data Center global observational database in three regions, including Russia, the Nordic countries, and Canada (Figure S7). Tables S6–S8 show the evaluation results in each region during each month of 2010 along with the benchmarks. Compared to the benchmarks, mean bias, gross error, and index of agreement could meet the criteria in most months, indicating the meteorology simulations in

this study are acceptable. The reasonable WRF performances ensure that there is no significant bias for the chemical transport modeling due to the meteorological fields.

2.3. Observations

2.3.1. Surface Black Carbon Measurement in the Arctic Circle

The BC concentrations simulated from H-CMAQ at the surface layer are evaluated against the ground-based measurements at various sites in the Arctic Circle. As of 2010, four Arctic sites had available black carbon data, including Barrow in Alaska (71.32°N, 156.62°W), Alert in Canada (82.5°N, 62.3°W), Zeppelin in Norway (78.9°N, 11.9°E), and Tiksi (71.59°N, 128.92°E) in Russia. The locations of the four sites are plotted in Figure 1b denoted by the red stars. All measurements are made by Aethalometer (AE-31, Magee Scientific Co.), and the conversion from aerosol absorption coefficient to BC concentration has been internally performed. It should be noted that the conversion from the measured aerosol absorption coefficient to BC mass concentration requires assumption of the mass absorption efficiency, which could be uncertain by a factor of 2 [*Stohl et al.*, 2013]. Black carbon measured from Aethalometer is referred to as Equivalent Black Carbon [*Petzold et al.*, 2013]. The concentrations measured at 520 nm are used for model verification in this study.

2.3.2. AERONET in Russia

Direct measurements of ambient BC concentrations are almost unavailable anywhere in Russia. In this regard, the aerosol inversion products from the Aerosol Robotic Network (AERONET) are used. AERONET is a global network measuring the aerosol optical properties using the ground-based Sun photometer [*Holben et al.*, 1998]. Aerosol size distribution, refractive index, and single scattering albedo were retrieved using sky radiance almucantar and direct Sun measurements [*Dubovik and King*, 2000]. Of all the aerosol inversion products, absorption aerosol optical depth (AAOD), which represents the total column extinction caused by light absorption, has been used as a surrogate for evaluation of the black carbon emissions [*Bond et al.*, 2013; *Koch et al.*, 2009]. AAOD is retrieved based on the single scattering albedo (ω_0), i.e., $\mathrm{AAOD} = \mathrm{AOD} \times (1 - \omega_0)$. Based on *Dubovik et al.* [2000], when AOD is lower than 0.2, the error of ω_0 is in the range of 0.05–0.07. As AOD increases, the error of ω_0 is lowered to 0.03. Considering that typical ω_0 values are in the range of 0.9–0.98, the accuracy of ω_0 is less than 8%. Thus, AAOD retrieved from AERONET is considered as a reliable aerosol product and could used as a benchmark for evaluation of the black carbon emissions. As of 2010, six AERONET sites were available in Russia, i.e., Moscow (55.7°N, 37.5°E), Zvenigorod (55.7°N, 36.8°E), Yekaterinburg (57.0°N, 59.5°E), Tomsk (56.5°N, 85.0°E), Yakutsk (61.7°N, 129.4°E), and Ussuriysk (43.7°N, 132.2°E). The locations of each site are also shown in Figure 1b denoted by the yellow circles.

Simulated AAOD is calculated by integrating the aerosol absorption coefficient ($\sigma_{ap}(z)$) with respect to altitudes (z), i.e.,

$$\mathrm{AAOD} = \int \sigma_{ap}(z) \cdot \mathrm{dz}\ , \text{ and } \sigma_{ap}(z) = 10.0 \times \mathrm{BC}(z), \tag{12}$$

BC(z) represents the simulated concentration ($\mu g\, m^{-3}$) at altitudes (z); 10.0 represents the empirical mass absorption efficiency ($m^2\, g^{-1}$) for BC.

3. Results and Discussion

3.1. Sectoral BC Emissions

The total anthropogenic BC emissions of Russia in 2010 are estimated to be 223.7 Gg based on the methodologies described in section 2.1. Figure 2 shows the percentage contributions of five emission sectors to the total. Gas flaring, residential emissions, and transportation are the three biggest contributors to Russia's total anthropogenic BC emissions with annual values of 81.0, 56.0, and 45.3 Gg, respectively. These three sectors contribute to emit 81.5% of Russia's total anthropogenic BC emissions. Emissions from industries and power plants are the least contributors, with annual values of 29.3 and 12.1 Gg, respectively.

Gas flaring unexpectedly ranks as the biggest source of BC emissions in Russia with a significant contribution of 36.2%. Globally, gas flaring only accounts for less than 3% of the black carbon emissions [*Stohl et al.*, 2013]. However, this source is significant for Russia as it is the world's largest gas flaring country as introduced in section 2.1.1. Currently, most global or regional emission inventories have not included emissions from gas flaring, possibly due to its low contribution at the global scale. However, at the regional scale, it could be significant as indicated in this study.

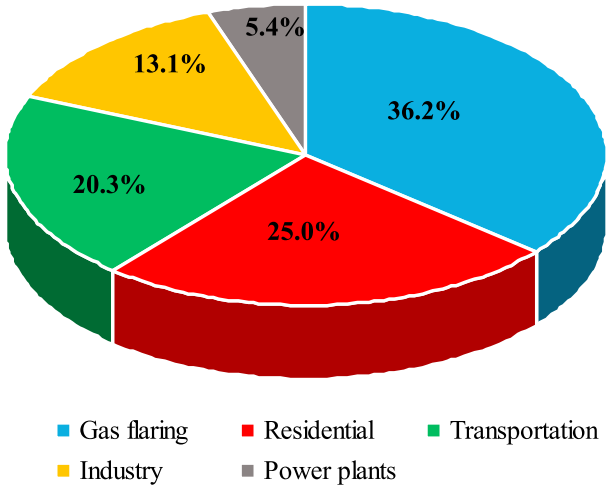

Figure 2. The percentage contributions of gas flaring, residential, transportation, industry, and power plants to Russia's total anthropogenic black carbon emission in 2010.

Residential BC emission is dominated by the usage of fuel wood and coal with contribution of ~95%. The contributions from other fuels are negligible due to either low consumptions or relatively low emission factors. The BC emission from fuel wood combustion reaches 34.2 Gg and contributes around 61% of the total residential BC emissions. Russia is in the world's top 10 countries for fuel wood consumption [*Food and Agriculture Organization*, 2012]. In areas where there is no gas network, and especially in the wood zones, fuel wood is the major fuel used in household (*EXPORT.BY*, 2009). Residential coal combustion contributes BC emission of 17.3 Gg. Compared to the coal combustion in the thermal power plants, its usage in household stoves is much less efficient due to the lower temperature during combustion with inadequate oxygen and also lack of effective emission control devices. Thus, the magnitude of residential coal combustion related BC emission is considerable.

On-road transportation BC emissions are dominated by private transportation, while the public transportation only contributes a minor percentage of 1.4%. Trucks (including heavy-duty and light-duty) contribute the most, at 65.7%, mainly due to the higher PM emission factors compared to the other vehicle categories and its relatively large stock number. Cars and private buses contribute 18.2% and 12.3% to the total road transportation BC emissions, respectively. Although cars possess the largest stock number among all the vehicle categories, their BC emissions are not so high. This is partly due to their relatively low PM emission factors and also the low percentage of black carbon in PM from gasoline combustion. The BC emission from warm-up is around 1.1 Gg.

Industrial activities from combustion in boilers contribute 13.1% to the Russian total anthropogenic BC emissions. Among the industrial subcategories, manufacture of coke/refined petroleum, metals products, wood products, and food products contribute most to the industrial BC emissions with the percentage of 20.6%, 18.5%, 18.4%, and 14.6%, respectively. For other industrial activities, their contributions are relatively small. Power generation and heating contributes only 5.4%. On the one hand, natural gas is the major fuel used for the thermal power plants in Russia, resulting in low BC emissions. On the other hand, there is no evidence indicating high BC emission factors from large coal-fired power plants due to common PM control practices.

3.2. Spatial Distribution

For the purpose of applying the new Russian emission inventory in atmospheric modeling, emissions are allocated based on the resolution of proxies and finally regrided to 0.1° × 0.1°. Figure 3 shows the spatial distributions of BC emissions for each sector.

Figure 3a shows the spatial distribution of BC emission from gas flaring. It clearly illustrates that the emissions are limited to specific regions. The Ural Federation District (location shown in Figure S5) in the Western Siberia is the region where the most intense gas flaring activities occur. As the largest natural gas and oil reserve and production base, the Ural Federation District accounts for over 50% of the whole nation's petroleum reserves [*Volkov*, 2008]. In this district, Khanty-Mansiysk and Yamal-Nenets (locations shown in Figure S2) are the major regions that contribute to gas flaring BC, with a few from Tomsk. The BC emission intensity over the intense gas flaring areas could reach up to 10 t/grid/yr (for grid size of 0.1° × 0.1°), which is the highest compared to the other emission sectors. In addition, the oil and gas fields at the conjunction areas of Komi and Nenets (Figure S2) also show relatively high intensities of BC emission from gas flaring although the areas of gas flaring are very limited. In some other regions of Russia, e.g., Orenburg, Irkutsk, Sakhalin, and part of the North Caucasian Federal District (Figure S2), some hot spots of gas flaring BC are also found, although their contributions compared to the Urals District are less.

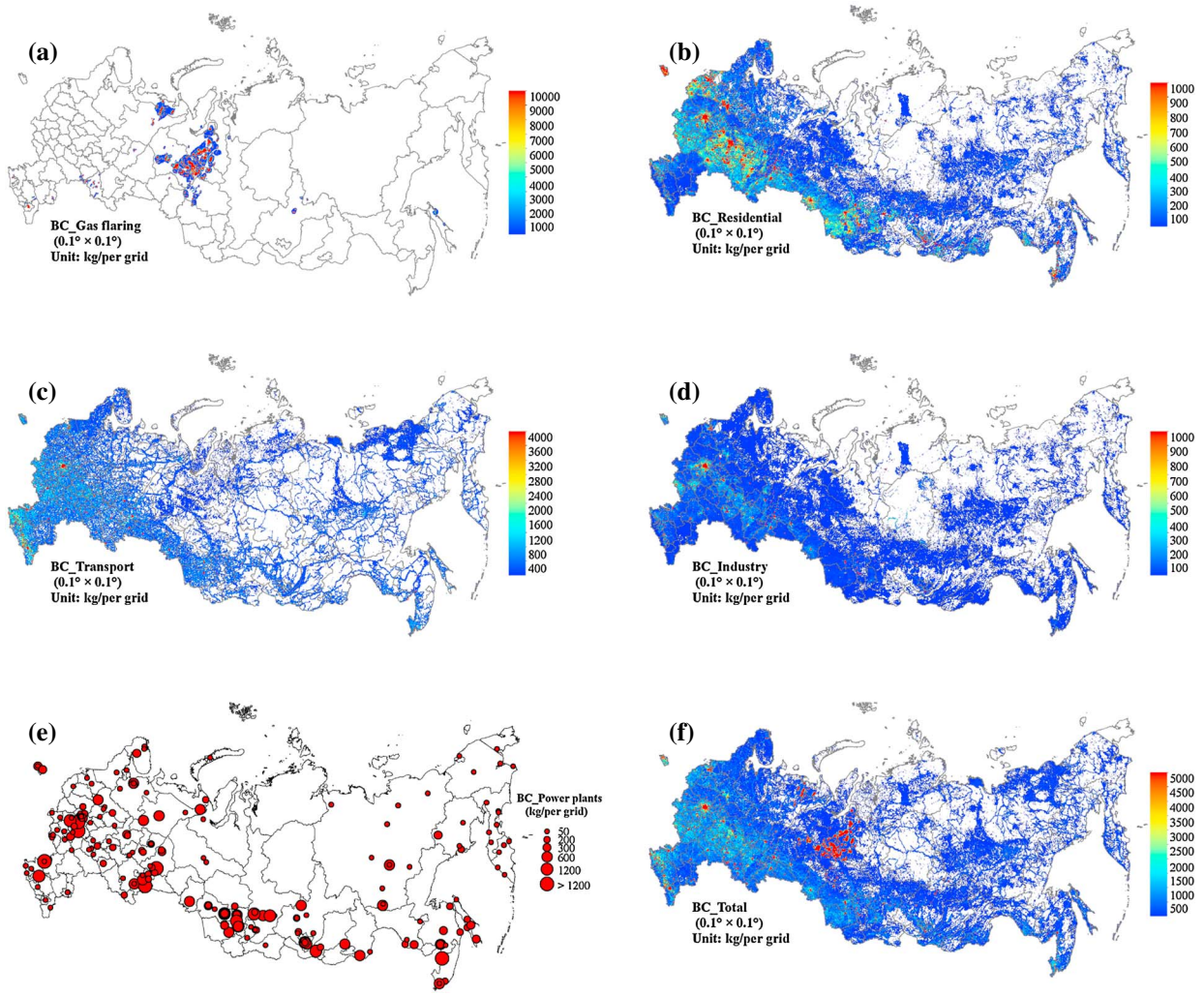

Figure 3. The spatial distribution of black carbon emission from (a) gas flaring, (b) residential, (c) transportation, (d) industries, (e) power plants, and (f) all combined emission sectors. The units are kg/per grid/yr, and the resolution of the grid cell is set as 0.1° × 0.1°.

Figure 3b shows the spatial distribution of residential BC emissions. The majority of the emissions are concentrated in the populated areas, e.g., the Central Federal District, the Volga Federal District, and southern part of the Urals and Siberian Federal District (see locations in Figure S5). Exceptions are found in the Southern Federal District and the North Caucasian Federal District, where the human population densities are the highest among the whole nation (Figure S4). Low fuel consumption in households over these regions is responsible for the low BC emissions there (Figure S5). In contrast, the Northwestern Federal District only possesses moderate human population density but shows hot spots over considerable areas. As indicated by Figure S5, the share of fuel wood consumption of the Northwestern Federal District is the highest in the nation. Colder weather in this area likely results in more fuel consumption in households and hence induces more black carbon emissions.

Figure 3c shows the spatial distribution of BC emission from transportation. Compared to the spatial distribution of human population density (Figure S4), the transportation BC emission tends to distribute around the populated areas. Hot spots are mainly observed in the big cities, e.g., Moscow, St. Petersburg, Novosibirsk, and Yekaterinburg.

Figure 3d shows the spatial distribution of industrial BC emissions. It is obvious that the industrial BC emissions are highly related to the spatial distribution of population density due to the spatial allocation method used in this study (section 2.1.5). The European part of Russia is the region where most industrial

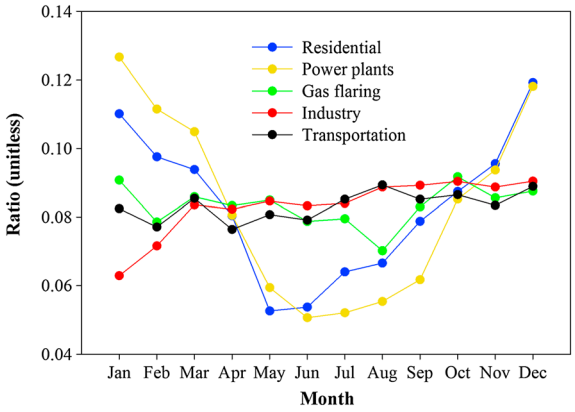

Figure 4. The monthly variation of normalized emissions for each sector.

emissions are found. It is also found that some remote areas, e.g., the central part of the Ural and the Siberian Federation District, show sparse hot spots.

Figure 3e shows the spatial distribution of BC emission from power plants. The European part of Russia with relatively dense human population obviously shows higher BC emissions due to more demands of electricity and heating in these regions. Also, the southern part of Russia shows considerable amounts of BC emission from power plants, including the southern Siberian Federal District and the southern Far Eastern Federal District. Although the Urals Federal District is the main base of natural gas and oil production, which requires a large amount of electrical power, low BC emissions from the power sector are found there. This is because most of the thermal power plants in that region use natural gas as the major fuel, which has negligible BC emissions.

At last, Figure 3f shows Russia's total anthropogenic BC emission by combining all the emission sectors referred above. Overall, high BC emission intensities occur in three major regions. The European part of Russia is the region where moderate/intense BC emissions spread over most areas. Human activities are the major emission sources as the majority of Russian people dwell in this region. In total, the BC emission from the European part of Russia (including Northeastern, Central, Volga, Southern, and North Caucasian Federal Districts; see Figure S5) reaches 103.6 Gg, accounting for 46.3% of the national totals. Of which, residential, transportation, and industries are the three major sources, accounting for 37.9%, 27.3%, and 23.6%, respectively. Besides the European part of Russia, the southern central part of Russia, mainly in the Siberian Federal District, also shows some hot spots, which are mainly located in those big cities. Another high-BC-intensity region is the northern part of the Ural Federal District. Total BC emission in the Ural Federal District reaches 77.7 Gg, accounting for 34.7% of the national totals. Of which, 90.7% is contributed by gas flaring. The BC emission intensities in the eastern part of Russia are overall low, mainly due to the low human population density and less human activities over these remote areas.

3.3. Monthly Pattern

Temporal allocations of sectoral emissions are important for achieving reasonable performance of chemical transport modeling. In this study, we derive the monthly profile of each emission sector according to their representative activity data reported by Russia's FSSS. Figure 4 shows the monthly variation of normalized emissions for each sector. The residential and power sectors present relatively strong monthly variations. On reaching the high values from January to March, the percentages of monthly residential BC emissions are lowest from May to June, then gradually increase and reach the highest value in December. The power sector shows more evidence of a seasonal pattern with higher values in the cold season (January–March and November–December) and lower values in the warm season (April–October). The behavior of the monthly variations of residential and power emissions are more related to human activities as the cold winter in Russia usually requires more fuel consumptions for electricity and heating. As for the other three sectors, i.e., gas flaring, industries, and transportation, their monthly profiles do not vary distinctly and are more evenly distributed throughout the year. Industrial activities are less influenced by the seasonal cycle compared to the residential and power sectors. The seasonal cycle of gas flaring is also relatively flat. As for transportation, although the emissions from the cold starts strongly depend on ambient temperature, their contribution to the total on-road transportation BC emissions is small. Hence, the BC emission from transportation is also not impacted much by the seasonal cycle.

Table 7 summarizes the monthly BC emissions by each sector and the combination of all sectors. Generally, the total anthropogenic BC emissions are lower from May to August. Relatively high BC emissions occur in January–March and October–December. The ratio of the BC emission between maxima and minimum is 1.37.

Table 7. Monthly Anthropogenic Emissions in Russia in 2010 (Units: Gg/month)

Sector	Jan	Feb	Mar	Apr	May	Jun	Jul	Aug	Sep	Oct	Nov	Dec
Gas flaring	7.4	6.4	7.0	6.8	6.9	6.4	6.4	5.7	6.7	7.4	6.9	7.1
Residential	6.2	5.5	5.3	4.5	2.9	3.0	3.6	3.7	4.4	4.9	5.4	6.7
Transportation	3.7	3.5	3.9	3.5	3.7	3.6	3.9	4.0	3.9	3.9	3.8	4.0
Industry	1.8	2.1	2.5	2.4	2.5	2.4	2.5	2.6	2.6	2.7	2.6	2.7
Power plants	1.5	1.3	1.3	1.0	0.7	0.6	0.6	0.7	0.7	1.0	1.1	1.4
Total	20.6	18.8	19.8	18.1	16.7	16.0	17.0	16.7	18.4	19.9	19.8	21.9

3.4. Comparison With Previous Studies and Emission Uncertainties

A regional BC emission inventory specifically developed for Russia is not available in previous studies; thus, it is only feasible to compare this work with emission inventories on the global or continental scale. *Bond et al.* [2004] developed a technology-based global inventory of carbonaceous aerosol from fossil fuels and biofuels considering the combinations of emission factors, fuel, combustion type, and control technologies. The emission factors used in their study are mostly based on the measurements of United States, e.g., U.S. EPA AP-42 and other parts of world while very few from the former Soviet Union countries. The major difference between this study and previous studies is the utilization of most recent Russian local information, e.g., composition-dependent gas flaring emission factor, local traffic emission factor, and local raw PM emissions with removal efficiency for certain sectors.

Based on *Bond et al.* [2007], the anthropogenic Russian BC emission was around 110 Gg in 2000. Without accounting for gas flaring, our study shows an estimate of 143 Gg for 2010. Considering an increase of fuel consumption from 2000 to 2010, higher BC emissions are expected. In *Wang et al.* [2011], the 2009 BC emission of Russia is simply doubled to be 220 Gg based on the 2000 emission [*Bond et al.*, 2007] for the purpose of matching the BC surface observations in the Arctic using Goddard Earth Observing System Chemistry (GEOS-Chem). Although this value is close to the total anthropogenic BC emission of 224 Gg in this study, it is obviously overestimated. Because the earlier studies [*Bond et al.*, 2007, 2004] did not account for gas flaring, a doubling of the emissions will not enhance emissions in areas where significant sources are missing. Thus, although the model simulation fits well against the observations in the Arctic [*Wang et al.*, 2011, 2014], this is an indication that the BC emissions in the other regions of Russia, except the gas flaring region, were over-tuned. A similar situation was found in the Regional Emission inventory in ASia (REAS) [*Kurokawa et al.*, 2013]. In REAS 2.1, the 2008 BC emission in the Urals of Russia is only 18 Gg, more than 3 times lower than this study due to the omission of gas flaring emissions. Since REAS only deals with the Asian part of Russia, it is difficult to compare with this study on both the national and sectoral scales. Until now, the only emission inventory with the inclusion of gas flaring emissions is the ECLIPSE (Evaluating the CLimate and Air Quality ImPacts of ShortlivEd Pollutants) project version 4.0 developed by the Greenhouse gas-Air pollution Interactions and Synergies model (http://gains.iiasa.ac.at). The gas flaring emission of ECLIPSE is included in the energy sector, and in 2010 it reaches around 57 Gg with the application of gas flaring emission factor of 1.6 g/m^3 [*Stohl et al.*, 2013]. However, the derivation of this gas flaring emission factor is not explicitly explained in *Stohl et al.* [2013]. Our study shows more than 40% higher gas flaring BC emission than the ECLIPSE estimate. Since both studies use the same activity data, emission factor is the only parameter influencing the result. In this study, the gas flaring emission factor is derived from the hydrocarbon composition of Russian local oil and gas mining fields and is assumed to be more representative. It is also noted that temporal distribution of gas flaring emission in ECLIPSE is assumed constant throughout the year [*Stohl et al.*, 2013] while we apply an activity-based temporal profile which will be better used for the chemical transport modeling presented below. For the other sectors in ECLIPSE, the 2010 BC emissions from residential, transportation, power (derived from energy minus gas flaring), and industry are 22.4, 52.0, 20.6, and 5.64 Gg/yr, respectively. The BC emissions from transportation are relatively close between this study and ECLIPSE. While for the residential and industry sector, this study is about 33 and 23 Gg/yr higher. For the power sector, this study is about 8 Gg/yr lower. ECLIPSE has an additional sector of agriculture waste of 24.6 Gg/yr. It should be noted that this study does not attempt to build any biomass burning-related emissions but will use the community biomass burning emission inventory (e.g., GFEDv4s in this study) as input for modeling. However, it is well known that GFED (and also other biomass burning emission inventories using the remote sensing technique) underestimates small fires such as agricultural

burning [*Randerson et al.*, 2012]. Thus, the agriculture waste sector from ECLIPSE is thought to be an important input to the biomass burning emission. Overall, the ECLIPSE data set yields an annual BC emission of 182.2 Gg, about 42 Gg lower than this study. The difference is mainly due to the discrepancies from the gas flaring, residential, and industrial emission sectors.

To obtain the uncertainties of this newly developed BC emission inventory, the Monte Carlo simulation is applied considering uncertainties from emission factors and activity data (e.g., fuel consumption and vehicle mileage traveled). Uncertainties from emission factors refer to the abated emission factors by assuming the penetration of control measures is certain. Emission factors are assumed to follow the lognormal distribution [*Bond et al.*, 2004]. Based on *Qin and Xie* [2011], the coefficient of variability (CV) for local emission factors is assumed to be 50%, e.g., the transportation sector in this study. The CV of the gas flaring BC emission factor is determined to be 68% based on the different composition of associated gas during the three stages of operation in the fields. While the CV for nonlocal emission factors largely increase, e.g., 150% for the residential sector with no local emission factors available [*Qin and Xie*, 2011]. As for the power, industrial and transportation sectors, the emission source fractions of BC in PM are used to scale the PM emissions. Based on the 32 BC profiles of coal-fired power plants from the U.S. Environmental Protection Agency SPECIATE database, a lognormal distribution is fitted. For the BC profiles in the industrial sector, a uniform distribution is used [*Zhao et al.*, 2011]. As for the transportation sector, the uncertainties of $BC/PM_{2.5}$ profiles [*EEA*, 2013b] are in the range of 5–50% depending on vehicle types and Euro standards. The uniform distribution is also applied to the transportation sector. Activity data are assumed to follow the normal distribution [*Zhao et al.*, 2011]. Twenty percent CV is assumed for residential consumption [*Qin and Xie*, 2011]. Ten percent CV is assumed for the vehicle mileage traveled (VMT) in the transportation sector [*Kioutsioukis et al.*, 2004]. As for the gas flaring volume, the error is determined to be 3.988 bcm for the year 2010 (http://ngdc.noaa.gov/eog/interest/flare_docs/BCM_Global_20110223.xlsx), yielding a CV of around 11%.

Based on the above assumptions of input data, the Monte Carlo simulation is conducted with 10,000 iterations for all five emission sectors. The uncertainties (95% confidence intervals around the central estimates) of BC emissions for the gas flaring, residential, transportation, industrial, and power plant sector are estimated to be −60%–240%, −69%–330%, −53%–136%, −44%–48%, and −79%–383%, respectively. Figure S8 shows the histogram of the results for Russia's total anthropogenic BC emissions combining all five emission sectors above. The values of the 2.5% and 97.5% are 91.6 and 1004.9 Gg, respectively, corresponding to an uncertainly level of −59.1%–349.2%.

3.5. Verification of the New Russian Black Carbon Emission Inventory by Model Simulation

Before examining how the model will perform by incorporating the new Russian BC emission inventory over both the Russian territory and the Arctic Circle, it is essential to evaluate the model performance over some major emission source regions at first. The continental United States, Europe, and China are chosen to be evaluated as they are the major source regions of global BC emissions. For the U.S., the Interagency Monitoring of Protected Visual Environments network (http://vista.cira.colostate.edu/improve) is available for a long-term measurement of aerosol chemical species, including the 2010 year of this study with 167 sites. For Europe, five sites in 2010 are available from the EBAS database (http://ebas.nilu.no/Default.aspx) developed and operated by the Norwegian Institute for Air Research, including sites of Harwell in the UK, Payerne in Switzerland, Palaiseau in France, Finokalia in Greece, and Preila in Lithuania. In addition, measurements from five background sites in Finland are included, but the data are average concentrations from December 2004 to December 2008 [*Hyvarinen et al.*, 2011]. As for China, we use the EC measurements from 18 stations of the China Atmosphere Watch Network operated by the Chinese Meteorological Administration, but it should be noted that all measurements were made in 2006 [*Zhang et al.*, 2008].

Figure 5 compares the 2010 annual mean BC concentrations between H-CMAQ simulation and observations in the continental United States, Europe, and China. The Mean Normalized Bias (MNB) defined as below is used to diagnose the model performance: $\mathrm{MNB} = \frac{1}{N}\sum_{i=1}^{N}\frac{C_m - C_o}{C_o} \times 100\%$, where C_m and C_o are the simulated and observed values at site *i*. The MNB for U.S. is +8.3%, indicating a very satisfactory model performance and the model only slightly overestimates the BC concentrations. For Europe and China, underestimations are found with MNB values of −29.3% and −25.9%, respectively. Our results are similar to the results

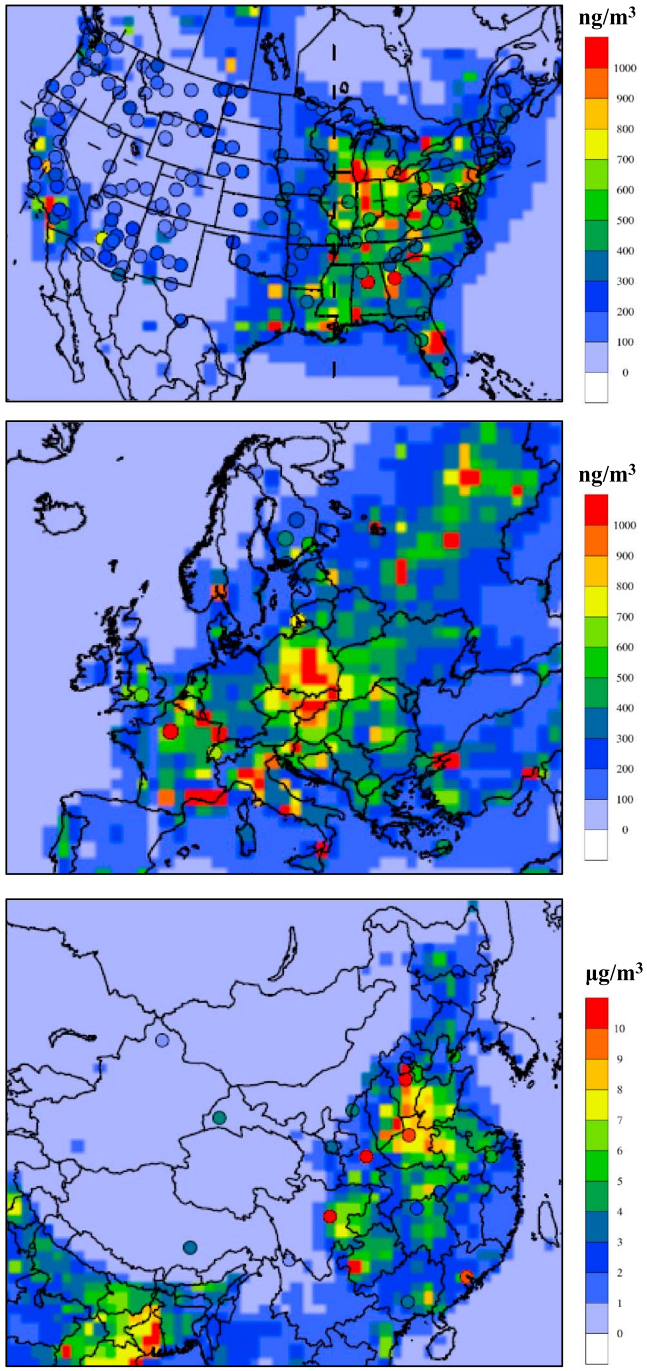

Figure 5. Comparison of 2010 annual mean BC concentrations between H-CMAQ simulation (contours) and the measurements (circles) made in the continental U.S., Europe, and China, respectively.

using GEOS-Chem for BC simulations in Europe and China, showing that BC concentrations were underestimated around 30% [*Wang et al.*, 2011, 2014].

Overall, our results suggest that the hemispheric version of CMAQ has good capability in reproducing the spatial distributions and magnitudes of BC aerosol in regions where emission inventories are built on relatively reliable information. Hence, this excludes the possibility that the discrepancy between the model simulation and observation in Russia and the Arctic that will be discussed below is due to the model configuration itself.

3.5.1. Simulation of AAOD in Russia

Two H-CMAQ simulations are conducted, one (hereinafter called "Base simulation") using the 2010 EDGAR-HTAPv2 global emission inventory and the other one using the same emission but with the Russian part superseded by the new Russian BC emission reconstructed in this study (hereinafter called "RUS simulation").

Comparison results between simulated and observed AAOD at six AERONET sites in Russia are shown in Figure 6. Note that no data are available for January, November, and December for all sites with some other months missing at different sites. It should also be noted that uncertainties may increase for the AAOD retrieval from AERONET when AOD values are less than 0.4 [*Holben et al.*, 2006]. Based on observations, distinct seasonal patterns are found at various sites. For example, Moscow shows the highest AAOD in August. Zvenigorod shows peaks in September and October. The other four sites all show higher AAOD values around February to April. Yekaterinburg and Yakutsk also show peaks in August and October, respectively. Generally, the model could well reproduce the site-specific monthly patterns as shown in Figure 6. However, the Base simulation strongly underestimates the monthly AAOD at all sites. On average, AAOD values are underestimated by 50%, 52%, 56%, 38%, 55%, and 29% at Zvenigorod, Moscow, Yekaterinburg, Tomsk, Yakutsk, and Ussuriysk, respectively. Compared to the Base simulation, the RUS simulation using the newly developed Russian BC emissions obviously improves the model performance by enhancing the site-specific AAOD values at different extents. At Zvenigorod, Moscow, Yekaterinburg, and Tomsk, their AAOD values are mostly enhanced by 65%, 62%, 39%, and 30%, respectively, under the RUS simulation. These four sites are all located in big cities

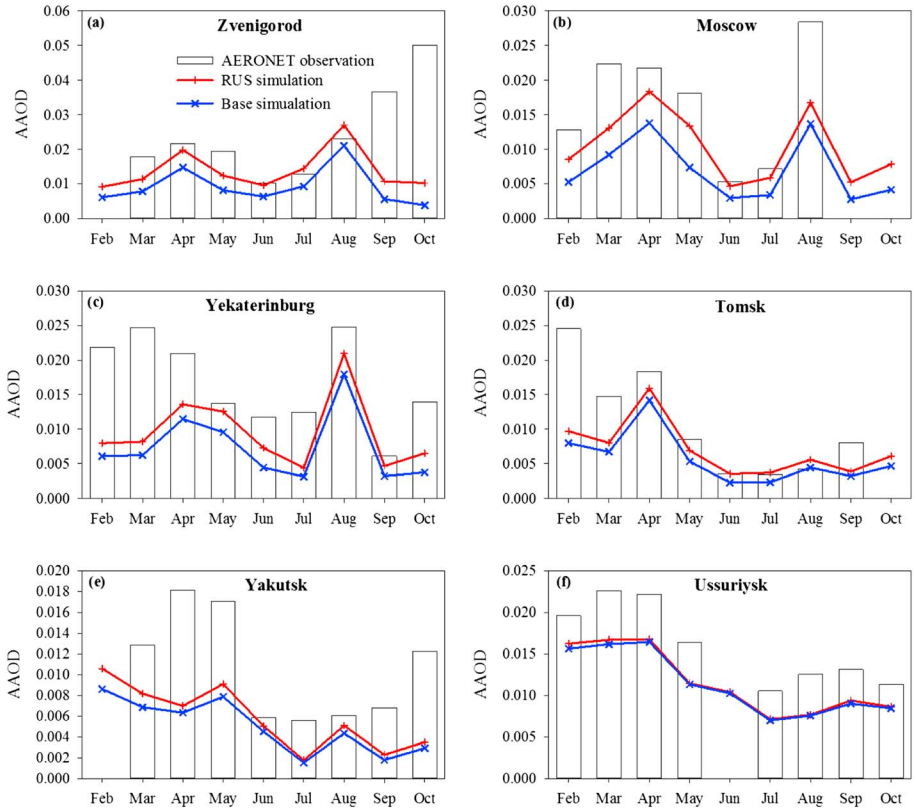

Figure 6. Comparison of monthly AAOD (absorption aerosol optical depth) between observations at six AERONET sites in Russia (white bar) and simulations from H-CMAQ modeling. The blue line (Base simulation) denotes the simulation using the 2010 EDGAR-HTAPv2 global emission inventory, and the red line (RUS Simulation) denotes the simulation using the same emission but with the Russian part superseded by the new emission created in this study.

of Russia, suggesting that the BC emissions in the dense population areas of Russia are highly underestimated in EDGAR-HTAPv2. While at the other two remote sites, much smaller improvement of AAOD values are achieved for Yakutsk and Ussuriysk of 18% and 3%. At Yakutsk, it could be found that AAOD values are still significantly underestimated throughout the whole year in spite of using the new Russian BC emission inventory. Underestimated regional transport could be one possible cause. Also, some missing sources are probably not accounted into the new emission inventory. Yakutsk is a major port on the Lena River, and the city's connection to the highway (Lena Highway) is only accessible by ferry in summer. Hence, shipping activities may contribute to the city's emissions. In addition, the region (the Republic of Sakha) that Yakutsk belongs to is rich in minerals such as gold, tin, mica, ferrous antimony, zeolitic, apatite, and oil-and-gas. Yakutsk itself is responsible for a fifth of the world's production of diamonds. Hence, mining activities (mainly from diesel heavy-duty machineries) may also contribute to the model underestimation. We believe that this situation could be ubiquitous in regions where mining industries are active and the transportation of goods relies on inland water shipping. Future work should account for emissions from mining and quarrying activities. Also, emissions from both domestic shipping and international shipping around the Arctic need to be updated. As for Ussuriysk, although AAOD is least underestimated by the model simulation among all sites, it still implied that local emissions could have been underestimated. On the other hand, almost no difference is observed between the Base and RUS simulations. As a small city with around 160,000 human population, its local emissions are not expected to be high as indicated by Figure 3f. However, its geographic location is very close to Northeast China (Figure 1b) where emission intensities are strong. Thus, the Chinese emission probably contributed to a considerable portion of the BC level at Ussuriysk, and this could explain why the new Russian BC emission inventory only shows small improvement of simulated AAOD at this site.

Overall, we find that the model performance using the new Russian BC emissions inventory is acceptable as compared to AAOD measured at six AERONET sites in Russia. However, the model does not perform well

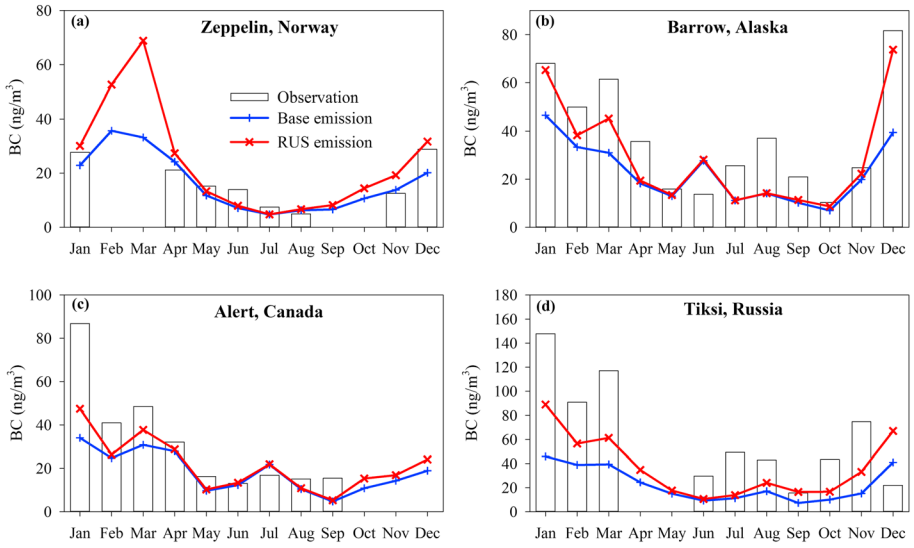

Figure 7. Comparison of monthly surface BC concentrations (ng/m^3) between observations at four Arctic sites and simulations from H-CMAQ modeling. The meanings of bar and lines are the same as Figure 6.

during certain months, e.g., September and October in Zvenigorod, February and March in Yekaterinburg, February in Tomsk, and all months in Yakutsk. This suggests that more efforts to determine local information such as activity data, emission factors, and temporal profiles are needed. In addition, the only public measurement network available in Russia is AERONET, which can measure the property of aerosol absorption, a proxy of ambient BC concentrations. The quantitative relationship between AAOD and BC varies depending on region, emission sources, environmental conditions, etc. Also, uncertainties exist for the inversion products of AERONET. Thus, direct measurements of BC in Russia are preferred to be used for the assessment of Russia's BC emissions in the future.

3.5.2. Simulation of Surface BC in the Arctic Circle

An important task of this study is to investigate how the new Russian emission inventory would improve the model performance of BC simulation over the Arctic Circle. Previous studies have shown that various models showed very poor capabilities of reproducing surface BC magnitudes and seasonal patterns over the Arctic Circle [*Koch et al.*, 2009; *Liu et al.*, 2011; *Shindell et al.*, 2008]. As similar as in section 3.5.1, we also compare the simulation results from the Base and RUS simulations to the BC observations over the Arctic Circle. The four Arctic sites are Zeppelin in Norway, Barrow in Alaska of the United States, Alert in Canada, and Tiksi in Russia (see locations in Figure 1b). In contrast to the AERONET network, which measures the absorption aerosol optical depth integrated for the whole atmospheric column, observations at these four sites are all measurements of equivalent BC concentration (units: ng/m^3) near the ground surface.

The results are presented in Figure 7. Generally, larger gaps between the two simulations are found in the cold seasons, i.e., January to March and November to December, when the Arctic haze mostly happens with higher BC concentrations. For other months from April to October, the differences between the two simulations are insignificant. This is mainly attributed to the different transport patterns in different seasons. In the cold seasons, the Siberian High tends to force the air from south to north into the Arctic [*Macdonald et al.*, 2005], thus bringing more BC emissions northward in the RUS simulation compared to the Base simulation. In the warm seasons, the continental high pressure disappears while oceanic low pressure weakens, resulting in weakening of the northward transport [*Macdonald et al.*, 2005].

Notable improvement from the RUS simulation is found at the Zeppelin site as shown in Figure 7a. February and March are the two months with highest BC concentrations. In the Base simulation, the modeled BC concentrations are 35.7 and 33.2 ng/m^3 in February and March, respectively. As a comparison, the RUS simulation could enhance the BC concentration of 17.0 and 35.7 ng/m^3, in turn, a dramatic increase of 48% and 107%. Unfortunately, observations during these two months in 2010 are not available, thus making the effect of improved BC emission on the model performance ambiguous. However, results in other months

could still shed some light. For example in December, the Base simulation predicts BC concentration of 20.2 ng/m^3, about 30% lower than the measured value of 28.8 ng/m^3. While the RUS simulation increases about 57% to 31.7 ng/m^3, which is fairly close to the observation. Observed BC concentrations during the warm season when boreal biomass burning are active, e.g., in June and July, are underestimated about 35–45%. As shown in Figure S9a, the contribution of biomass burning to the monthly mean surface BC concentration in June ranges from 2.8 to 4.5 ng/m^3 based on three biomass burning inventories, i.e., GFEDv4s, GFASv1.0, and FINNv1.5. While in July, contributions from biomass burning are less than 1 ng/m^3. It is possible that the negative model biases in these months are partly ascribed to the underestimation of biomass burning emission inventories as they all rely on the remote sensing technique, which has weaker capability of detecting small fires and may miss fire spots under meteorological conditions such as overcast and precipitation.

At Barrow (Figure 7b), the Base simulation exhibits an average of 38% underestimation during the first three months from January to March. By using the new Russian BC emission, the simulated BC could be increased about 34%. The most polluted month of 2010 at Barrow is December with an average BC concentration of 81.6 ng/m^3. The Base simulation only simulates 39.4 ng/m^3, which is way off from the observation with more than 50% underestimation. After performing the RUS simulation, the modeled BC concentration in December is dramatically enhanced by about 90% to 73.8 ng/m^3, much closer to the observed value. In June, the model significantly overestimates 60–105%. Contributions from biomass burning range from 16.5 to 22.8 ng/m^3 and overwhelm that of 5.4 ng/m^3 from the nonbiomass burning emissions (Figure S9b). This is likely due to the overestimated biomass burning from boreal North America. However, the model underestimates BC concentrations observed in the following three months and biomass burning contributes moderate fractions of 8–39%. In this regard, it is possible that biomass burning emissions in these months could have been underestimated.

As for Alert (Figure 7c), the impact of the increased Russian BC emissions on this site is not as significant as the other three sites. During the cold seasons (January to March and October to December), the RUS simulation has a moderate improvement of around 26% compared to the Base simulation. The most significant underestimation is found in January, when BC is underestimated about 45% even under the RUS simulation. Similar to the study by *Stohl et al.* [2013], which introduced the gas flaring emission and domestic emission with an improved temporal profile, BC concentrations are also significantly underestimated at Alert during the cold seasons. However, unlike the systematic underestimation in all months of the cold season (January–May and November–December) in *Stohl et al.* [2013], this study demonstrates that the strong underestimation in January at Alert seems exceptional. Possible missing or underestimated sources in the remote areas of Canada may account for this. Also, the transport from source areas to Alert could be underestimated if the modeled atmospheric removal of BC particles is more rapid than the actual removal.

The worst model performance is found for the Tiksi site. The Base simulation significantly underestimates the BC concentrations by 67% throughout the whole year. Under the RUS simulation, simulated BC concentrations are enhanced by 75% during the cold seasons (January to March and November to December). However, the BC concentrations at Tiksi are still underestimated about 45%. In the other months (April to October), the RUS simulation also shows an evident enhancement of about 45%; however, the simulated BC concentrations are still underestimated about 47%. As we compare the simulation results between Tiksi and Yakutsk (Figure 6e), similar strong underestimations are found at both of the two remote sites. Modeled atmospheric removal of particles may be too rapid over these remote areas. Also, the simulation suggests that the local emissions in the remote areas of Russia are not well represented. Unaccounted emissions from mining and quarrying activities in the remote Far East may be partly responsible for this. Tiksi is located at the Arctic Ocean coast of the remote Far East and serves as one of the principal ports for accessing the Laptev Sea. Shipping emission is possibly another responsible source as this sector is not updated in this study. In addition, it should be noted that the East Arctic Shelf near Tiksi is an offshore reserve of natural gas and oil [*Volkov*, 2008]. Unaccounted gas flaring emissions from possible offshore mining activities may also explain the underestimated BC concentrations at Tiksi. At last, biomass burning emissions contribute to BC concentrations from less than 1 ng/m^3 to 6.7 ng/m^3 in the warm seasons, accounting for 4–44% of the simulated concentrations (Figure S9d). *Konovalov et al.* [2014] uses a top-down method and shows that the biomass burning CO_2 emissions in Siberia are a factor of 2.5 and 1.8 larger than estimates from GFEDv3.1 and GFASv1.0. In this regard, the significantly underpredicted BC levels in Tiksi are probably partly due to the underestimation of Siberia biomass burning emissions.

Overall, based on the model evaluation of AAOD/BC at six Russian AERONET sites and four remote Arctic sites, the newly reconstructed Russian BC emission inventory shows evident improvement for modeling black carbon over the Arctic Circle. Although the model performance is not satisfactory everywhere, confidence is gained that improving Russia's emission inventory can increase the capability of models in reproducing ambient black carbon over the Arctic region. This study not only provides the atmospheric modeling community a more representative Russian black carbon emission inventory but also points out that the role of Russia's emissions on the Arctic haze could have been significantly underestimated in past studies. It should be noted that this study does not intend to apportion the contribution of different emission sectors or regions to the Arctic haze. This apportionment will be investigated in the future study.

4. Conclusions

A high-resolution ($0.1° \times 0.1°$) regional anthropogenic BC emission inventory is developed for the Russian Federation. Activity data from combination of local Russian information and international resources, emission factors from either Russian documents or adjusted values for local conditions, and other emission source data are used to approximate the BC emissions. As of 2010, total anthropogenic BC emission in Russia is estimated to be around 223.7 Gg. The uncertainty level of this Russian BC emission inventory is in the range of −59.1%–349.2% (95% confidence level) by using the Monte Carlo simulation. Based on laboratory scale experiment of flared gases and chemical composition of flared gases from oil and gas fields in Russia, a gas flaring BC emission factor representative of Russia is estimated to be 2.27 g/m^3. It should be noted that this gas flaring BC emission is extrapolated beyond the experimental range and needs further verification from real-life flare measurement. Based on the DMSP satellite retrievals, Russia ranks as the biggest gas flaring country in 2010. Recently, by using the Visible Infrared Imaging Radiometer Suite (VIIRS) on board the Suomi National Polar Partnership satellite [*Elvidge et al.*, 2013], both spatial resolution and detection limits of flares have been significantly improved. Although the calibration for estimating flared gas volumes from the VIIRS data is still in progress, it is expected that more accurate information on global gas flaring will be obtained. In this study based on the available activity data and estimated emission factor, BC emissions from gas flaring account for a significant percentage of 36.2% in Russia's total anthropogenic BC emissions. However, this sector has been often neglected in various global/regional emission inventories. Residential BC emissions contribute 25.0% dominated by the usage of fuel wood and coal. Transportation, industry, and power plants contribute 20.3%, 13.1%, and 5.4% to the total, respectively. Compared to previous studies, the gas flaring sector shows the largest discrepancy, more than 40% higher than ECLIPSE which is the only emission inventory that considers gas flaring emissions until now. As for the nonflaring total anthropogenic sources, the results in this study are within the previous other estimates. High BC emission intensities are mainly found in three regions. The European part of Russia and the southern central part of Russia are two of them due to the relatively high human population densities there. Although the Urals Federal District only possesses very sparse human population, the BC emission intensity in this region is the highest in Russia due to its intense gas flaring activities. An activity-based monthly profile is developed. Residential and power sectors exhibit relatively strong temporal variation with higher values in winter and spring. Other sectors, i.e., gas flaring, industry, and transportation, have relatively steady monthly trends.

Hemispheric CMAQ with a polar stereographic projection is applied to simulate the ambient BC over the northern hemisphere. Two sets of emissions are used as inputs for the model, i.e., EDGAR-HTAPv2 and EDGAR-HTAPv2 with its Russian part replaced by the newly developed Russian BC emissions in this study. Comparisons between simulations using these two emission inventories and observations indicate obvious improvement of simulated BC in both Russia and the Arctic Circle. At four AERONET sites located in big cities of Russia, the simulation using the new Russian BC emission inventory could improve 30–65% of AAOD, a proxy of BC, throughout the whole year compared to the simulation using the EDGAR-HTAPv2 inventory. However, the improvement is moderate at remote sites, suggesting possible unaccounted emissions. Over the Arctic Circle, surface BC simulations are mostly improved during the Arctic haze periods (October–March). The most notable improvement is achieved at the Zeppelin site. Dramatic increases of 48% (17.0 ng/m^3) and 107% (35.7 ng/m^3) of the monthly mean BC concentrations are found in February and March, respectively. At Barrow, the modeled BC concentration in December is enhanced by almost 90% to 73.8 ng/m^3, much closer to the observed value of 81.6 ng/m^3. As for Alert, a moderate improvement of around 26% is achieved during the cold seasons (January to March and October to December). Although

the worst model performance is found at the Tiksi site, simulated BC concentrations are enhanced by 75% during the cold seasons by using the new Russian BC emission inventory. Improvement of model performance is mainly attributed to the following factors: (1) increased magnitudes of Russian BC emissions; (2) more accurate spatial distribution of BC emissions, e.g., the added gas flaring emission; and (3) application of the activity-based temporal profile.

This study presents a comprehensive perspective of the shortcomings of the current available BC emissions of Russia. We find that the biased Russian BC emission is one of the most important reasons that chemical transport models are struggling to reproduce the BC levels over the Arctic. It is pointed out that the role of Russia's emissions on the Arctic haze could have been significantly underestimated. However, simulation with the new Russian BC emission input still underestimates the BC concentrations either near the surface over the Arctic or the total atmospheric columns in Russia. Apart from possible transport issues in the model, considerable uncertainties still exist in the current emission inventory due to the constraints of information we have. For instance, information of associated gas composition dependent on various fields is essential for more accurately estimating the gas flaring emissions. This may require the sharing of information from the oil and gas companies that have operations in different fields. Field sampling and laboratory measurements with sufficient samples are needed to characterize the composition of associated gases. Also, laboratory measurements of gas flaring emission factors based on high calorific fuels are especially needed. Unavailability and poor quality of local emission factors and activity data are ubiquitous in most of Russia's emission sectors. For instance, splits of the gasoline and diesel consumption for the onroad transportation are not available. Emission factors of heavy fuels used in the Russian power plants are unknown. Unaccounted emission sectors in this study such as nonroad transportation need special attention in the future works. *Evans et al.* [2015] estimates that the mining industry contributes the largest fraction of 69% to the BC emissions from diesel sources in the Murmansk Oblast. This may partly explain the negative biases of the model simulation in those remote areas that are active in mining and quarrying activities. In addition, current Russian emission methodology still focuses on particulate matter without size differentiation (i.e., total suspended particles) but not $PM_{2.5}$ which is more harmful to human health and subject to long-range transport. At last, although not the main focus of this study, various community biomass burning emission inventories are found underestimated in the boreal regions, and this could explain part of the negative biases of simulated BC. Overall, this study should be considered as a starting point for establishing Russia's BC emission inventory. Continuous and additional research works in Russia are needed to strengthen the understanding of the role of Russia's emissions on the atmospheric chemistry and climate over the Arctic.

Acknowledgments

This work is supported by Interagency Acquisition Agreement S-OES-11_IAA-0027 from the U.S. Department of State to the U.S. Department of Energy. John M. Storey and Vitaly Y. Prikhodko were supported by the U.S. Department of Energy and performed at Oak Ridge National Laboratory (ORNL). ORNL is managed by UT-Battelle, LLC, for the U.S. Department of Energy under contract DE-AC05-00OR22725. The computational resources used in this work are supported by the University of Tennessee and Oak Ridge National Laboratory Joint Institute for Computational Sciences (http://www.jics.tennessee.edu). UT-Battelle owns the copyright of the LandScan 2010™ High Resolution global Population Data Set (http://www.ornl.gov/landscan/). We sincerely thank Vitaly Y. Prikhodko's coordination with SRI Atmosphere to obtain part of the emission source data used in this study, NOAA NGDC for providing the global gas flaring volumes and nighttime products, HTAPv2 for accessing the global air pollutants emissions, NOAA for archiving BC measurement data in the Arctic, the principal investigators of AERONET in Russia for establishing and maintaining all the sites, and Алексей Филиппов (Alexey Filippov) for publishing the data of associated gas composition of Russia in the website www.avfinfo.ru. We greatly thank for Yanfen Lin for assisting the GIS technique. This work does not reflect the official views or policies of the United States Government or any agency thereof, including the funding entities. The mention of any computer software, data products, and or computational hardware does not represent endorsement by the authors nor organizations that the authors are associated with. The Russian black carbon emission source data generated in this study can be obtained via http://abci.ornl.gov/download.shtml (ABCI: Arctic Black Carbon Initiative) or http://acs.engr.utk.edu/Data.php (Air Quality Engineering & Climate Studies Research Group, University of Tennessee, Knoxville). We sincerely thank for three anonymous reviewers' constructive comments on greatly improving the quality of this paper.

References

Amann, M., Z. Klimont, and F. Wagner (2013), Regional and global emissions of air pollutants: Recent trends and future scenarios, *Annu. Rev. Environ. Resour.*, *38*, 31–55, doi:10.1146/annurev-environ-052912-173303.

Arctic Monitoring and Assessment Programme (AMAP) (2011), The impact of black carbon on Arctic climate. Written by P.K. Quinn, A. Stohl, A. Arneth, T. Berntsen, J. F. Burkhart, J. Christensen, M. Flanner, K. Kupiainen, H. Lihavainen, M. Shepherd, V. Shevchenko, H. Skov, and V. Vestreng. Arctic Monitoring and Assessment Programme (AMAP), Oslo. 72 pp.

Andreae, M. O., and P. Merlet (2001), Emission of trace gases and aerosols from biomass burning, *Global Biogeochem. Cycles*, *15*(4), 955–966, doi:10.1029/2000GB001382.

Banks, J. (2012), Best practices for reduction of methane and black carbon from Arctic oil and gas production, the publication of the Clean Air Task Force, Published: July 2012. [Available at http://www.catf.us/resources/publications/view/170.]

Bond, T. C., D. G. Streets, K. F. Yarber, S. M. Nelson, J. H. Woo, and Z. Klimont (2004), A technology-based global inventory of black and organic carbon emissions from combustion, *J. Geophys. Res.*, *109*, D14203, doi:10.1029/2003JD003697.

Bond, T. C., E. Bhardwaj, R. Dong, R. Jogani, S. K. Jung, C. Roden, D. G. Streets, and N. M. Trautmann (2007), Historical emissions of black and organic carbon aerosol from energy-related combustion, 1850–2000, *Global Biogeochem. Cycles*, *21*, GB2018, doi:10.1029/2006GB002840.

Bond, T. C., et al. (2013), Bounding the role of black carbon in the climate system: A scientific assessment, *J. Geophys. Res. Atmos.*, *118*, 5380–5552, doi:10.1002/Jgrd.50171.

Byun, D., and K. L. Schere (2006), Review of the governing equations, computational algorithms, and other components of the models-3 Community Multiscale Air Quality (CMAQ) modeling system, *Appl. Mech. Rev.*, *59*(1–6), 51–77, doi:10.1115/1.2128636.

Canadian Association and Petrolium Producers (CAPP) (2007), *A Recommended Approach to Completing the National Pollutant Release Inventory (NPRI) for the Upstream Oil and Gas Industry*, Canadian Association and Petrolium Producers, Calgary, Canada.

Chen, Y. J., G. R. Zhi, Y. L. Feng, D. Y. Liu, G. Zhang, J. Li, G. Y. Sheng, and J. M. Fu (2009), Measurements of black and organic carbon emission factors for household coal combustion in China: Implication for emission reduction, *Environ. Sci. Technol.*, *43*(24), 9495–9500, doi:10.1021/Es9021766.

Cheng, M. D. (2014), Geolocating Russian sources for Arctic black carbon, *Atmos. Environ.*, *92*, 398–410, doi:10.1016/j.atmosenv.2014.04.031.

Christensen, J. H. (1997), The Danish Eulerian hemispheric model - A three-dimensional air pollution model used for the Arctic, *Atmos. Environ.*, *31*(24), 4169–4191, doi:10.1016/S1352-2310(97)00264-1.

Dubovik, O., and M. D. King (2000), A flexible inversion algorithm for retrieval of aerosol optical properties from Sun and sky radiance measurements, *J. Geophys. Res.*, *105*(D16), 20,673–20,696, doi:10.1029/2000JD900282.

Dubovik, O., A. Smirnov, B. N. Holben, M. D. King, Y. J. Kaufman, T. F. Eck, and I. Slutsker (2000), Accuracy assessments of aerosol optical properties retrieved from Aerosol Robotic Network (AERONET) Sun and sky radiance measurements, *J. Geophys. Res.*, *105*(D8), 9791–9806, doi:10.1029/2000JD900040.

EEA (2013a), EMEP/EEA air pollutant emission inventory guidebook 2013, Part B: Sectoral guidance chapters: 1.A.1 Energy industries, European Environment Agency, published on Aug 29, 2013.

EEA (2013b), EMEP/EEA air pollutant emission inventory guidebook 2013, Part B: sectoral guidance chapters: 1.A.3.b. i-iv Exhaust emissions from road transport, European Environment Agency, published in August 29, 2013.

Elvidge, C. D., D. Ziskin, K. E. Baugh, B. T. Tuttle, T. Ghosh, D. W. Pack, E. H. Erwin, and M. Zhizhin (2009), A fifteen year record of global natural gas flaring derived from satellite data, *Energies*, *2*(3), 595–622, doi:10.3390/En20300595.

Elvidge, C. D., M. Zhizhin, F. C. Hsu, and K. E. Baugh (2013), VIIRS nightfire: Satellite pyrometry at night, *Remote Sens.*, *5*(9), 4423–4449, doi:10.3390/Rs5094423.

Evans, M., and V. Roshchanka (2014), Russian policy on methane emissions in the oil and gas sector: A case study in opportunities and challenges in reducing short-lived forcers, *Atmos. Environ.*, *92*, 199–206, doi:10.1016/j.atmosenv.2014.04.026.

Evans, M., N. Kholod, V. Malyshev, S. Tretyakova, E. Gusev, S. Yu, and A. Barinov (2015), Black carbon emissions from Russian diesel sources: Case study of Murmansk, *Atmos. Chem. Phys.*, *15*, 8349–8359, doi:10.5194/acp-15-8349-2015.

EXPORT.BY (2009), Modern technologies of use of biomass in Russia. [Available at http://export.by/en/?act=s_docs&mode=view&id=1856&type=&mode2=archive&doc=64.]

Food and Agriculture Organization (2012), *FAO Yearbook of Forest Products 2010 (ISSN 1020-458X)*, Food and Agriculture Organization of the United Nations, Rome.

Filippov, A. (2012), [Available at http://www.avfinfo.ru/page/inzhiniring-006] (in Russian), posted on May 12, 2012.

FSSS (2011), Federal State Statistics Service, Russia in Figures: Section 1. Basic social and economic indicators by regions of the Russian Federation. [Available at http://www.gks.ru/bgd/regl/b11_12/IssWWW.exe/Stg/d01/01-05-2.htm.]

Grammelis, P., N. Koukouzas, G. Skodras, E. Kakaras, A. Tumanovsky, and V. Kotler (2006), Refurbishment priorities at the Russian coal-fired power sector for cleaner energy production - Case studies, *Energy Policy*, *34*(17), 3124–3136, doi:10.1016/j.enpol.2005.06.009.

Hirdman, D., H. Sodemann, S. Eckhardt, J. F. Burkhart, A. Jefferson, T. Mefford, P. K. Quinn, S. Sharma, J. Ström, and A. Stohl (2010), Source identification of short-lived air pollutants in the Arctic using statistical analysis of measurement data and particle dispersion model output, *Atmos. Chem. Phys.*, *10*, 669–693, doi:10.5194/acp-10-669-2010.

Holben, B. N., et al. (1998), AERONET - A federated instrument network and data archive for aerosol characterization, *Remote Sens. Environ.*, *66*(1), 1–16, doi:10.1016/S0034-4257(98)00031-5.

Holben, B. N., T. F. Eck, I. Slutsker, A. Smirnov, A. Sinyukc, J. Schaferc, D. Gilesc, and O. Dubovik (2006), AERONET's version 2.0 quality assurance criteria, *Proc. SPIE*, *6408*, 64080Q, doi:10.1117/12.706524.

Huang, K., J. S. Fu, E. L. Hodson, X. Dong, J. Cresko, V. Y. Prikhodko, J. M. Storey, and M. D. Cheng (2014), Identification of missing anthropogenic emission sources in Russia: Implication for modeling Arctic haze, *Aerosol Air Qual. Res.*, *14*(7), 1799–1811, doi:10.4209/aaqr.2014.1708.0165.

Huang, L., S. L. Gong, C. Q. Jia, and D. Lavoue (2010), Importance of deposition processes in simulating the seasonality of the Arctic black carbon aerosol, *J. Geophys. Res.*, *115*, D17207, doi:10.1029/2009JD013478.

Hyvarinen, A. P., et al. (2011), Aerosol black carbon at five background measurement sites over Finland, a gateway to the Arctic, *Atmos. Environ.*, *45*(24), 4042–4050, doi:10.1016/j.atmosenv.2011.04.026.

International Energy Agency (IEA) (2012), *CO2 Emissions from Fuel Combustion (2012 edition)*, International Energy Agency, OECD, Paris, doi:10.1787/co2_fuel-2012-en.

Izrael, Y. A., et al. (1997), Russian Federation climate change country study final report, volume 1: Inventory of technogenic GHG emissions (Cooperative agreement DE-FCO2-93PO10118), Russian Federal Service for Hydrometeorology and Environmental Monitoring, Moscow, 1997.

Johnson, M. R., R. W. Devillers, and K. A. Thomson (2011), Quantitative field measurement of soot emission from a large gas flare using Sky-LOSA, *Environ. Sci. Technol.*, *45*(1), 345–350, doi:10.1021/Es102230y.

Johnson, M. R., R. W. Devillers, and K. A. Thomson (2013), A generalized Sky-LOSA method to quantify soot/black carbon emission rates in atmospheric plumes of gas flares, *Aerosol Sci. Technol.*, *47*(9), 1017–1029, doi:10.1080/02786826.02782013.02809401.

Junker, C., and C. Liousse (2008), A global emission inventory of carbonaceous aerosol from historic records of fossil fuel and biofuel consumption for the period 1860–1997, *Atmos. Chem. Phys.*, *8*(5), 1195–1207, doi:10.5194/acp-8-1195-2008.

Kioutsioukis, I., S. Tarantola, A. Saltelli, and D. Gatelli (2004), Uncertainty and global sensitivity analysis of road transport emission estimates, *Atmos. Environ.*, *38*(38), 6609–6620, doi:10.1016/j.atmosenv.2004.08.006.

Klimont, Z., J. Cofala, I. Bertok, M. Amann, C. Heyes, and F. Gyarfas (2002), Modelling particulate reductions in Europe: A framework to estimate reduction potential and control costs, Interim Report (IR-02-076), International Institute for Applied Systems Analysis (IIASA), Laxenburg, Austria.

Koch, D., et al. (2009), Evaluation of black carbon estimations in global aerosol models, *Atmos. Chem. Phys.*, *9*(22), 9001–9026.

Konovalov, I. B., E. V. Berezin, P. Ciais, G. Broquet, M. Beekmann, J. Hadji-Lazaro, C. Clerbaux, M. O. Andreae, J. W. Kaiser, and E.-D. Schulze (2014), Constraining CO2 emissions from open biomass burning by satellite observations of co-emitted species: A method and its application to wildfires in Siberia, *Atmos. Chem. Phys.*, *14*, 10,383–10,410, doi:10.5194/acp-14-10383-2014.

Kupiainen, K., and Z. Klimont (2007), Primary emissions of fine carbonaceous particles in Europe, *Atmos. Environ.*, *41*(10), 2156–2170, doi:10.1016/j.atmonsenv.2006.10.066.

Kurokawa, J., T. Ohara, T. Morikawa, S. Hanayama, G. Janssens-Maenhout, T. Fukui, K. Kawashima, and H. Akimoto (2013), Emissions of air pollutants and greenhouse gases over Asian regions during 2000–2008: Regional Emission inventory in ASia (REAS) version 2, *Atmos. Chem. Phys.*, *13*(21), 11,019–11,058, doi:10.5194/acp-13-11019-2013.

Laing, J. R., P. K. Hopke, E. F. Hopke, L. Husain, V. A. Dutkiewicz, J. Paatero, and Y. Viisanen (2014), Long-term particle measurements in Finnish Arctic: Part II Trend analysis and source location identification, *Atmos. Environ.*, *88*, 285–296, doi:10.1016/j.atmosenv.2014.01.015.

Law, K. S., and A. Stohl (2007), Arctic air pollution: Origins and impacts, *Science*, *315*(5818), 1537–1540, doi:10.1126/science.1137695.

Li, X. H., S. X. Wang, L. Duan, J. M. Hao, and Y. F. Nie (2009), Carbonaceous aerosol emissions from household biofuel combustion in China, *Environ. Sci. Technol.*, *43*(15), 6076–6081, doi:10.1021/Es803330j.

Liu, J. F., S. M. Fan, L. W. Horowitz, and H. Levy (2011), Evaluation of factors controlling long-range transport of black carbon to the Arctic, *J. Geophys. Res.*, *116*, D04307, doi:10.1029/2010JD015145.

Macdonald, R. W., T. Harner, and J. Fyfe (2005), Recent climate change in the Arctic and its impact on contaminant pathways and interpretation of temporal trend data, *Sci. Total Environ.*, *342*(1–3), 5–86, doi:10.1016/j.scitotenv.2004.12.059.

Mathur, R., R. C. Gilliam, R. Bullock, S. J. Roselle, J. E. Pleim, D. C. Wong, F. S. Binkowski, and D. G. Streets (2012), Extending the applicability of the Community Multiscale Air Quality model to hemispheric scales: Motivation, challenges, and progress, in *Air Pollution Modeling and its Application XXI*, *NATO Science for Peace and Security Series C: Environmental Security*, vol. 4, edited by D. G. Steyn and S. Trini Castelli, Springer, Dordrecht, Netherlands, doi:10.1007/978-94-007-1359-8_30.

McEwen, J. D. N., and M. R. Johnson (2012), Black carbon particulate matter emission factors for buoyancy-driven associated gas flares, *J. Air Waste Manage. Assoc.*, *62*(3), 307–321, doi:10.1080/10473289.10472011.10650040.

Ministry of Transport of the Russian Federation Research Institute (MTRFRI) (2008), Ministry of Transport of the Russian Federation Research Institute, Instructions on the inventory of emissions of motor vehicles into the air (in Russian). Расчетная инструкция (методика) по инвентаризации выбросов загрязняющих веществ автотранспортными средствами в атмосферный воздух.

Nguyen, Q. T., H. Skov, L. L. Sorensen, B. J. Jensen, A. G. Grube, A. Massling, M. Glasius, and J. K. Nojgaard (2013), Source apportionment of particles at Station Nord, North East Greenland during 2008–2010 using COPREM and PMF analysis, *Atmos. Chem. Phys.*, *13*(1), 35–49, doi:10.5194/acp-13-35-2013.

Office of Technological and Environmental Surveillance (2005), Requirements for approvals and settlement fees for environmental pollution: Calculation of emissions into the air from stationary sources of pollution, Approved by the Deputy Head of the Office of Technological and Environmental Surveillance in the Primorsky Territory on January 1, 2005 (in Russian) Требования к прохождению согласований платежейи расчетам платыза загрязнение окружающей природной среды, Утверждены зам. руководителя Управления по технологическому и экологическому надзору по Приморскому краю Бибиковым М.Н. 01 января 2005 года.

Pearson, P., S. Bodin, L. Nordberg, and A. Pettus (2013), On thin ice: How cutting pollution can slow warming and save lives: Main report. A Joint Report of The World Bank and The International Cryosphere Climate Initiative, Washington D. C., World Bank. [Available at http://documents.worldbank.org/curated/en/2013/10/18496924/thin-ice-cutting-pollution-can-slow-warming-save-lives-vol-1-2-main-report.]

Petzold, A., et al. (2013), Recommendations for reporting "black carbon" measurements, *Atmos. Chem. Phys.*, *13*(16), 8365–8379, doi:10.5194/acp-13-8365-2013.

PFC Energy (2007), Using Russia's associated gas, Prepared for the Global Gas Flaring Reduction Partnership and the World Bank.

Qin, Y., and S. D. Xie (2011), Estimation of county-level black carbon emissions and its spatial distribution in China in 2000, *Atmos. Environ.*, *45*(38), 6995–7004, doi:10.1016/j.atmosenv.2011.09.017.

Quinn, P. K., G. Shaw, E. Andrews, E. G. Dutton, T. Ruoho-Airola, and S. L. Gong (2007), Arctic haze: Current trends and knowledge gaps, *Tellus, Ser. B*, *59*(1), 99–114, doi:10.1111/j.1600-0889.2006.00238.x.

Rahn, K. A. (1981), Relative importances of North-America and Eurasia as sources of arctic aerosol, *Atmos. Environ.*, *15*(8), 1447–1455, doi:10.1016/0004-6981(81)90351-6.

Randerson, J. T., Y. Chen, G. R. van derWerf, B. M. Rogers, and D. C. Morton (2012), Global burned area and biomass burning emissions from small fires, *J. Geophys. Res.*, *117*, G04012, doi:10.1029/2012JG002128.

Sand, M., T. K. Berntsen, O. Seland, and J. E. Kristjansson (2013), Arctic surface temperature change to emissions of black carbon within Arctic or midlatitudes, *J. Geophys. Res. Atmos.*, *118*, 7788–7798, doi:10.1002/Jgrd.50613.

Schaap, M., H. A. C. D. Van Der Gon, F. J. Dentener, A. J. H. Visschedijk, M. Van Loon, H. M. ten Brink, J. P. Putaud, B. Guillaume, C. Liousse, and P. J. H. Builtjes (2004), Anthropogenic black carbon and fine aerosol distribution over Europe, *J. Geophys. Res.*, *109*, D18207, doi:10.1029/2003JD004330.

Sharma, S., M. Ishizawa, D. Chan, D. Lavoue, E. Andrews, K. Eleftheriadis, and S. Maksyutov (2013), 16-year simulation of Arctic black carbon: Transport, source contribution, and sensitivity analysis on deposition, *J. Geophys. Res. Atmos.*, *118*, 943–964, doi:10.1029/2012JD017774.

Shaw, G. E. (1995), The arctic haze phenomenon, *Bull. Am. Meteorol. Soc.*, *76*(12), 2403–2413, doi:10.1175/1520-0477(1995)076<2403:Tahp>2.0.Co;2.

Shindell, D. T., et al. (2008), A multi-model assessment of pollution transport to the Arctic, *Atmos. Chem. Phys.*, *8*(17), 5353–5372.

SRI-Atmosphere (2012), Review of existing method for assessment of emissions (PM/soot) used in Russia for major sources. Chapter 3.1. Calculation methods used in Russia to estimate PM/soot emissions from power plants and boilers (in Russian), St. Petersburg, 2012.

Stohl, A. (2006), Characteristics of atmospheric transport into the Arctic troposphere, *J. Geophys. Res.*, *111*, D11306, doi:10.1029/2005JD006888.

Stohl, A., Z. Klimont, S. Eckhardt, K. Kupiainen, V. P. Shevchenko, V. M. Kopeikin, and A. N. Novigatsky (2013), Black carbon in the Arctic: The underestimated role of gas flaring and residential combustion emissions, *Atmos. Chem. Phys.*, *13*(17), 8833–8855, doi:10.5194/acp-13-8833-2013.

Streets, D. G., S. Gupta, S. T. Waldhoff, M. Q. Wang, T. C. Bond, and Y. Y. Bo (2001), Black carbon emissions in China, *Atmos. Environ.*, *35*(25), 4281–4296, doi:10.1016/S1352-2310(01)00179-0.

USEPA (1995), *AP-42—Compilation of Air Pollutant Emission Factors*, vol. I, 5th ed.—Section 13.5 ed., USEPA, U.S. Environmental Protection Agency, Research Triangle Park, NC.

van der Werf, G. R., J. T. Randerson, L. Giglio, G. J. Collatz, M. Mu, P. S. Kasibhatla, D. C. Morton, R. S. DeFries, Y. Jin, and T. T. van Leeuwen (2010), Global fire emissions and the contribution of deforestation, savanna, forest, agricultural, and peat fires (1997–2009), *Atmos. Chem. Phys.*, *10*(23), 11,707–11,735, doi:10.5194/acp-10-11707-2010.

Volkov, D. (2008), Russian natural gas – A review, Edited by Dr. Michelle Michot Foss, Univ. of Texas - Austin, Bureau for Economics Geology, Center for Energy Economic.

Wang, H., R. C. Easter, P. J. Rasch, M. Wang, X. Liu, S. J. Ghan, Y. Qian, J. H. Yoon, P. L. Ma, and V. Vinoj (2013), Sensitivity of remote aerosol distributions to representation of cloud-aerosol interactions in a global climate model, *Geosci. Model Dev.*, *6*(3), 765–782, doi:10.5194/gmd-6-765-2013.

Wang, Q. Q., D. J. Jacob, J. R. Spackman, A. E. Perring, J. P. Schwarz, N. Moteki, E. A. Marais, C. Ge, J. Wang, and S. R. H. Barrett (2014), Global budget and radiative forcing of black carbon aerosol: Constraints from pole-to-pole (HIPPO) observations across the Pacific, *J. Geophys. Res. Atmos.*, *119*, 195–206, doi:10.1002/2013JD020824.

Wang, Q., et al. (2011), Sources of carbonaceous aerosols and deposited black carbon in the Arctic in winter-spring: Implications for radiative forcing, *Atmos. Chem. Phys.*, *11*(23), 12,453–12,473, doi:10.5194/acp-11-12453-2011.

Wheeler, D., and K. Ummel (2008), Calculating CARMA: Global estimation of CO2 emissions from the power sector. Center for Global Development, Working Pap. 145.

World Bank (2012), Estimated Flared Volumes from Satellite Data, 2007–2011. [Available at http://web.worldbank.org/WBSITE/EXTERNAL/TOPICS/EXTOGMC/EXTGGFR/0,,contentMDK:22137498~pagePK:64168445~piPK:64168309~theSitePK:578069,00.html.]

Zhang, X. Y., Y. Q. Wang, X. C. Zhang, W. Guo, and S. L. Gong (2008), Carbonaceous aerosol composition over various regions of China during 2006, *J. Geophys. Res.*, *113*, D14111, doi:10.1029/2007JD009525.

Zhao, Y., C. P. Nielsen, Y. Lei, M. B. McElroy, and J. Hao (2011), Quantifying the uncertainties of a bottom-up emission inventory of anthropogenic atmospheric pollutants in China, *Atmos. Chem. Phys.*, *11*(5), 2295–2308, doi:10.5194/acp-11-2295-2011.